Improved Accuracy of Watershed-Scale General Circulation Model Runoff Using Deep Neural Networks

Joshua S. Rice[1], Sheila M. Saia[1*], Ryan E. Emanuel[1,2]

[1]Department of Forestry and Environmental Resources, North Carolina State University, Raleigh, NC 27695, USA

[2]Center for Geospatial Analytics, North Carolina State University, Raleigh, NC 27695, USA

*Corresponding author: Sheila M. Saia (ssaia@ncsu.edu)

Key Points:

- We used a deep neural network (DNN) to predict watershed-scale runoff from gridded, downscaled general circulation model (GCM) outputs.
- The DNN reduced the error of runoff predictions from 51% for gridded GCM runoff to 29% for DNN watershed-scale runoff.
- The DNN outperformed other modeling methods used to convert downscaled GCM outputs to watershed-scale runoff.

This manuscript was submitted to Journal of Advances in Modeling Earth Systems (JAMES) for peer review on December 31, 2019. This document is a preprint. Supplemental information is included at the end of this document.

Abstract

Projecting impacts of climate change on water resources is a vital research task, and general circulation models (GCMs) are important tools for this work. However, the spatial resolution of downscaled GCMs makes them difficult to apply to non-grid conforming scales relevant to water resources management: individual watersheds. Machine learning techniques like deep neural networks (DNNs) may address this issue. Here we use a DNN to predict monthly watershed-scale runoff (i.e., stream discharge divided by watershed area) from monthly gridded and downscaled Coupled Model Intercomparison Project Phase 5 (CMIP5) GCM hydroclimatic fluxes (i.e., precipitation, evapotranspiration, and temperature). We used hydroclimatic fluxes, biotic, and abiotic characteristics from 2,731 watersheds in the conterminous United States to train and test a DNN that can predict watershed-scale runoff. The DNN described 93% (Pearson's correlation coefficient = 0.962) of the variability in observed runoff and was temporally and spatially robust. The median absolute error (MAE) of DNN predictions was approximately 25 percentage points lower than that of gridded, downscaled GCM runoff or monthly normal runoff (i.e., 30-year average of runoff observations at the watershed-outlet). DNN monthly runoff predictions had the lowest MAE of all the grid-to-watershed-scale conversion approaches we tested, including: linear ridge regression, support vector machines, extreme gradient boosting, and artificial neural networks. We demonstrated why using DNNs to convert gridded GCM hydroclimatic fluxes to watershed-scales is relevant to water resources research and management. We also provided a methods guide for hydrologists interested in implementing machine learning techniques.

Plain Language Summary

Environmental scientists use runoff from general circulation models (GCM) to study the impacts of climate change on water resources. One GCM grid square may represent runoff for a large area on Earth's surface (e.g., a 100km by 100km square). This coarse resolution and gridded nature of GCM outputs make them difficult to use at the watershed-scale because watersheds are rarely square-shaped. There are many ways to convert gridded GCM runoff to the watershed-scale, and machine learning techniques such as deep neural networks (DNNs) have yet to be applied to this task. Thus, we used a large, publicly available dataset to train a DNN to convert GCM outputs to watershed-scale runoff for 2,731 watersheds in the USA. The DNN accurately predicted watershed-scale runoff even when the runoff varied in space and time. The DNN outperformed all the grid-to-watershed-scale conversion approaches we tested. In summary, machine learning techniques like DNNs may help improve runoff predictions. These improved predictions may be especially helpful in regions of the USA experiencing climate change-induced drought (e.g., Colorado, USA) and flooding (e.g., North Carolina, USA). Finally, we discussed modeling best practices that may help environmental scientists interested in implementing DNN techniques.

Keywords

machine learning, deep neural networks, deep learning, downscaling, general circulation models, runoff

1 Introduction

Water is a critical resource for human society and ecosystems (Oki & Kanae, 2006; Zhao & Running, 2010; Srinivasan et al., 2017) and projecting the impacts of future climate change on water resources is a fundamental task for hydrologists and the larger scientific community (Vorosmarty et al., 2000; NRC, 2012; Blöschl et al., 2019). Tools such as general circulation models (GCM) help researchers investigate how watersheds respond to climate change (Chiew et al., 2009; Alkama et al., 2013; Zhang et al., 2014; Bring et al., 2015; Knighton et al., 2019). However, GCM outputs (e.g., precipitation, temperature, runoff) are gridded and typically have spatial resolutions measured on the order of degrees (e.g., 1.4° x 1.4° or ~150 km x ~120 km for the MIROC5 model at the T85 gridded resolution at 40°N 100°W; ENES, 2016), which may be too coarse for many watershed-scale investigations (Chiew et al., 2009). To overcome this issue, researchers rely on various methods to resolve—or downscale—coarser resolution GCM data to finer spatial resolutions (Fowler et al., 2007). To date, machine learning techniques such as deep neural networks (DNNs) have played a limited role in downscaling GCM outputs.

Downscaling techniques are typically grouped into either dynamical or statistical approaches (Hewitson & Crane, 1996; Fowler et al., 2007; Schoof, 2013). Dynamical downscaling nests higher resolution, physically-based, regional models within lower resolution GCMs where regional (or finer) observations constrain GCM boundary conditions (Hewiston & Crane, 1996; Chiew et al., 2009; Schoof, 2013). Dynamical downscaling requires considerable computational demand (Fowler et al., 2007; Chiew et al., 2009; Arritt & Rummukainen, 2011; Schoof, 2013) and outputs are often still gridded, albeit, at a finer resolution than the original GCM grid. Statistical downscaling uses regression models to relate lower resolution GCM output to higher resolution observations (Charles et al., 2004; Fowler et al., 2007; Chiew et al., 2009). Besides regression models, statistical downscaling methods may also include weather classifications and weather generators (Fowler et al., 2007; Schoof, 2013). Statistical downscaling can be less computationally demanding than dynamical downscaling and can generate downscaled GCM outputs at any grid scale as well as the (non-gridded) watershed-scale (Wilby & Wigley, 1997; Fowler et al., 2007). However, statistical downscaling requires data records of substantial length, can poorly predict extreme events, and can be hindered by non-stationarity (Wilby, 1997; Wilby & Wigley, 1997; Fowler et al., 2007).

Machine learning methods are not new to statistical GCM downscaling; however, there has been limited application of DNNs in this research area. Previous studies have used three major machine learning methods to downscale GCM data. They include support vector machines (SVMs; Tripathi et al., 2006; Ghosh et al., 2008; Guo et al., 2009), relevance vector machines (RVMs; Ghosh et al. 2008), and artificial neural networks (ANNs; Hewitson & Crane, 1996; Trigo & Palutikof, 1999; Cavazos, 2000; Sheridan & Lee 2011; Ramseyer et al., 2018). SVMs map input data into a high dimensional feature space and then classify data into groups by minimizing classification error to hyperplanes within this high dimensional space (Raghavendra et al., 2014). RVMs are similar to SVMs but rely on probabilistic Bayesian learning to classify data into groups (Ghosh et al., 2008). ANNs consist of layers of nodes (also called cells or neurons) and edges where each layer of nodes and edges represents a linear or non-linear input-output mapping (Shen, 2018). The values of ANN nodes and edges are adjusted during training to minimize a loss function that compares the ANN predicted output to the observed output (Dawson & Wilby, 1998; Shen, 2018). Besides being used to downscaled climate predictions via a regression-style approach (e.g., Trigo & Pulutikof; 1999), ANNs are used to develop self-organizing maps that aid statistical downscaling via weather typing schemes (e.g., Ramseyer et al., 2018). ANNs have up to four layers (Figure S1a) including an input layer, two hidden layers, and an output layer. In contrast, DNNs are extensions of ANNs containing more than two hidden layers (Figure S1b). We know of one study using convolutional neural networks (CNNs)—a class of DNNs applied to multiple two-dimensional inputs such as images—to develop seasonal and regional extreme weather classifications from gridded GCM outputs (Knighton et al., 2019). To the best of our knowledge, no studies have used DNNs to downscale gridded GCM runoff to the watershed-scale.

Machine learning-based downscaling methods offer benefits over other downscaling methods. Machine learning techniques such as DNNs are agnostic to the mathematical parameterization of physical processes, even though they may effectively recreate those processes from related data or be used in coordination with physically-based models (Shen, 2018; Shen et al., 2018). Rather, machine learning techniques assume that mathematical parameterizations of physical relationships are represented in observational data themselves (LeCun et al., 2015; Goodfellow et al., 2016; Shen, 2018; Shen et al., 2018). Consequently, DNNs may enable researchers to identify hydrologic processes that remain poorly characterized or even undiscovered, generate hypotheses, and conduct targeted field and/or physically-based hydrologic modeling studies based on these hypotheses (Shen et al., 2018). Given sufficiently large training datasets and model regularization—a process that relies on a loss function to simultaneously reward model accuracy and flexibility (Goodfellow et al., 2016)—DNNs can be more robust compared to other statistical approaches (i.e., regularized linear regression; Shen, 2018; Shen et al., 2018). In the context of GCM downscaling, a robust DNN is one that accurately predicts watershed-scale runoff from a test set of gridded GCM outputs across a spatio-temporal gradient. The test set includes observational data that was not used to train the model (see *Sections 2.2* and *4.5*).

Specific to downscaling, machine learning techniques offer a flexible approach to explore complex relationships between gridded GCM outputs, watershed characteristics, and watershed-scale runoff. DNNs, in particular, are well suited for downscaling because they have more hidden layers than ANNs. These extra hidden layers enable DNNs to (1) represent complex, non-linear relationships between inputs and outputs and (2) identify relationships in a high-dimensional space given limited initial parameterization (LeCun et al., 2015; Goodfellow et al., 2016; Knighton et al., 2019). The number of hidden layers (i.e., increased model depth) is not the only reason why DNNs are well suited for representing complex relationships between inputs and outputs; diverse model architectures, unsupervised pretraining, and weight sharing improve computational convergence in DNNs (Shen, 2018). Furthermore, neural network-based approaches may overcome temporal and spatial non-stationarity by enabling the incorporation of additional variables (Wilby & Wigly, 1997) such as time-lagged climate variables.

Machine learning techniques such as DNNs are not without limitations: time-efficient development require specialized computing resources (e.g., graphical processing units; GPUs), large amounts of data are a prerequisite, and machine learning techniques can be difficult to train due to vanishing gradients and the potential for model overfitting (Glorot & Bengio, 2010; Sutskever et al., 2013; Srivastava et al., 2014; He et al., 2015; Ioffe & Szegedy, 2015; Schmidhuber, 2015; Shen et al., 2018). In the case of GCMs, certain hydrologic processes may not be represented within the data and data may be temporally or spatially incomplete (Shen et al., 2018). Last, DNNs are often criticized for treating physical processes and/or relationships between variables as a black box (Shen et al., 2018). Despite these issues, a number of techniques can be implemented to achieve efficient DNN training and accurate DNN test set predictions (Goodfellow et al., 2016; Shen, 2018; Shen et al., 2018). Some of these techniques include: dropout (Srivastava et al., 2014), batch normalization (Ioffe & Szegedy, 2015), variance scaling of initial weights (He et al., 2015), early stopping (Goodfellow et al., 2016), and the use of semi-random sampling when holding out data for the test set (Rice et al., 2019). We discuss each in *Section 2.2*. Recent advances in optimization algorithms, computer hardware (e.g., GPUs), computer software (e.g., Google TensorFlow), and cloud computing services (e.g., Amazon Web Services' Sage Maker) have also made the utilization of machine learning methods readily feasible for applications in hydrology and other areas (LeCun et al., 2015; Schmidhuber et al., 2015; Shen et al., 2018). Furthermore, explanation techniques such as local interpretable model-agnostic explanations (LIME; Ribeiro et al., 2018; Worland et al., 2019), can help model developers assess the trustworthiness of their machine learning algorithm results.

Given the limited use of DNNs in hydrologic science and the practical need to generate watershed-scale runoff from GCMs, this study aims to demonstrate the application of DNNs to the practical problem of downscaling GCM runoff from grid cells to watersheds, which are fundamental units of hydrologic analysis. The objectives of this study are to: (1) train and test a DNN that accurately predicts watershed-scale runoff from gridded, downscaled GCM data and (2) compare DNN performance to alternative grid-to-watershed-scale conversion techniques.

This study also serves as a guide to hydrologists and other earth systems scientists who are interested in applying DNNs and other machine learning tools to their work.

2 Methods

2.1 Data Overview

We used the United States Geological Survey Geospatial Attributes of Gages for Evaluating Streamflow version II (GAGES-II) dataset, which provides standardized, continuous, long-term streamflow records and watershed characteristics (e.g., mean elevation and mean percent developed land cover) for watersheds across the United States (Falcone et al., 2010). We downloaded GAGES-II data from https://water.usgs.gov/GIS/metadata/usgswrd/XML/gagesII_Sept2011.xml#stdorder. More specifically, we identified 2,731 reference (i.e., un-disturbed watersheds, n = 558) and non-reference (i.e., human-disturbed, n = 2,173) watersheds in the conterminous United States (CONUS) with corresponding GAGES-II mean daily streamflow records that were ≥ 99% complete from January 1970 - December 1999 (Figure 1). We included both reference and non-reference watersheds to better reflect the increasingly pervasive effects of human activity on the hydrologic cycle (Dynesius & Nilsson, 1994; Nilsson et al., 2005; Villarini & Smith, 2010; Rice et al., 2015; Emanuel et al., 2015; Munoz et al. 2018). We downloaded streamflow data from https://water.usgs.gov and skipped approximately 10,200 observations at the beginning of the streamflow data time series in order to incorporate time-lagged features as discussed below. This resulted in a total of 972,960 monthly runoff observations from 2,731 separate watersheds. We converted daily streamflow from the GAGES-II dataset from discharge to runoff (i.e., mm) by dividing daily discharge by the watershed area, which we obtained from the GAGES-II dataset. We aggregated observed runoff from a daily mean, as provided in the GAGES-II dataset, up to a monthly mean and then used this monthly runoff as a response variable when training and testing the DNN (Figure S2).

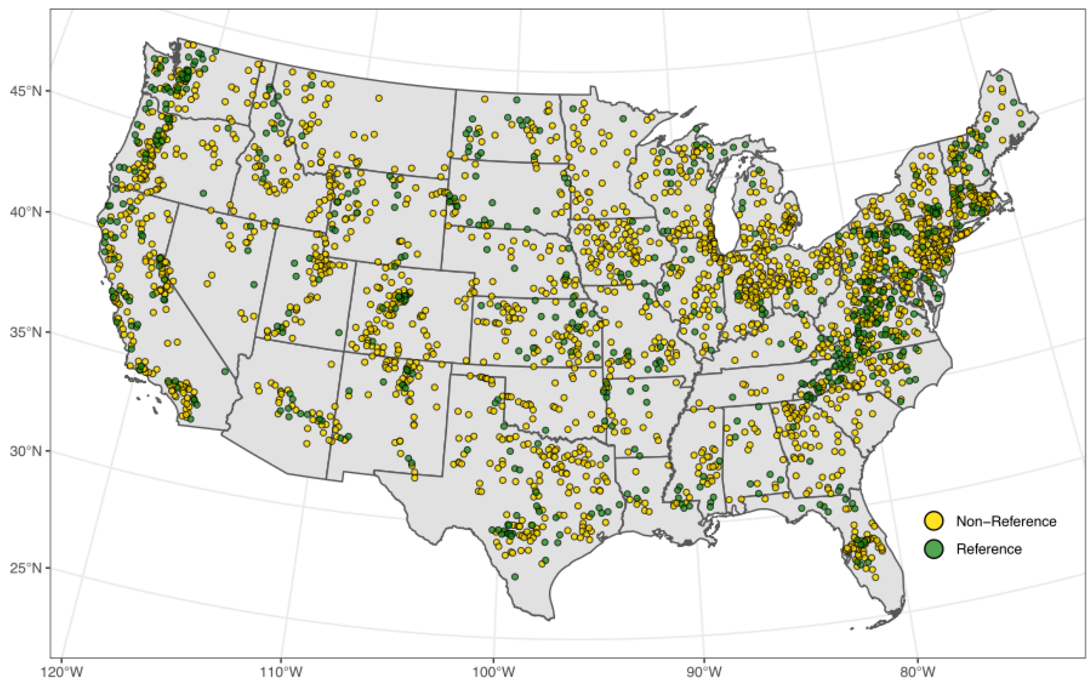

Figure 1. Location (centroid) of non-reference and reference watersheds included in this study.

We used GAGES-II watershed characteristics as DNN features (i.e., predictor variables) when training and testing the DNN; these variables addressed themes of climate, watershed topography, geomorphology, soil properties, and land cover. For a full description of the watershed characteristics included in this study, see Table S1. In addition to GAGES-II data, we downloaded monthly, gridded, downscaled precipitation, temperature, evapotranspiration, and runoff GCM outputs for each of the 2,731 study watersheds at a spatial resolution of 1/8° x 1/8°

(14 km x 11 km at 40°N 100°W) for the previously mentioned 30-year study period for an ensemble of 18 (model abbreviations: bcc_csm1-1, ccsm4, cesm1-cam5, csiro-mk3-6-0, fio-esm, gfdl-cm3, gfdl-esm2g, gfdl-esm2m, giss-e2-r, hadgem2-ao, hadgem2-es, ipsl-cm5a-lr, ipsl-cm5a-mr, miroc-esm, miroc-esm-chem, miroc5, noresm1-m, and noresm1-me) CMIP5 GCMs (Maurer et al., 2007; Taylor et al., 2012). We downloaded CMIP5 data from http://gdo-dcp.ucllnl.org/downscaled_cmip_projections/. We used temperature data from all 18 CMIP5 GCMs. For precipitation, evapotranspiration, and runoff data, we excluded ipsl-cm5a-lr and noresm1-me GCMs because they only provided annual averages over the study period (i.e., 1970-1999) and hydroclimatic fluxes (i.e., runoff) needed for model comparisons were not available. We used each watershed boundary to calculate a watershed areal average value (i.e., area weighted average of gridded GCM data falling within the watershed boundary) for each CMIP5 variable (i.e., temperature, precipitation, evapotranspiration, runoff) and each GCM. We then calculated the mean CMIP5 variable across GCMs for each watershed. This resulted in a monthly ensemble value, which we used for all remaining analyses. We also calculated the one-, two-, and three-month time lags in monthly average GCM ensemble precipitation, temperature, and evapotranspiration using a similar areal average approach (Table S1). We used the ArcGIS (version 10.4.1; ESRI, 2011) arcpy Python library to calculate watershed areal averages. Similar to the watershed characteristics discussed previously, we used the ensemble monthly average precipitation, temperature, and evapotranspiration (i.e., unlagged and lagged) as continuous features when training and testing the DNN (Figure S2). We compared model runoff predictions to ensemble monthly average runoff; thus, ensemble monthly average runoff served as a control (see *Section 2.4*).

2.2 Deep Neural Network Development, Architecture, & Testing

The combination of a 30-year study period and 2,731 study watersheds resulted in a total of 972,960 monthly observations of runoff that were ≥ 99% complete. We constructed the DNN train set by randomly sampling (i.e., 75% of observations from each ecoregion and either reference/non-reference class) observations at each time step (i.e., monthly) over the 30-yr study period. We refer to this grouped random selection as semi-random sampling; its purpose is to ensure that the trained DNN model can accurately represent non-random spatio-temporal autocorrelation in the original dataset by explicitly forcing consistent and complete spatio-temporal coverage (Rice et al., 2019). We used the remaining 25% of the data as a test set to assess model performance (i.e., DNN testing). For a complete breakdown of data included in the train and test sets see Figure S3. We used an NVIDIA GeForce GTX 1070 GPU (NVIDIA, Santa Clara, CA) on a desktop PC with a 3.5 GHz Intel Core i7-5820K central processing unit (CPU; Intel, Santa Clara, CA) and 32GB of memory to train the DNN. We carried out DNN training and testing in Python (version 3.7.1; Python Software Foundation, 2018) using the open source TensorFlow (version 1.12.0, https://www.tensorflow.org/, Abadi et al., 2015) and Keras (version 2.2.4, https://github.com/fchollet/keras, Chollet et al., 2015) software libraries.

We applied a number of techniques to counter issues such as poor network initializations and data over-fitting, which can both limit DNN performance. These techniques included: dropout, batch normalization, variance scaling of initial weights, and early stopping. *Dropout* is a computationally efficient way to combine many network structures and prevent over-fitting; it adds noise and limits co-dependencies between neurons during DNN training (Srivastava et al., 2014; Goodfellow et al. 2016). It involves temporarily removing randomly selected neurons during DNN training (Srivastava et al., 2014; Goodfellow et al., 2016; Worland et al. 2019). *Batch normalization* helps improve DNN training efficiency and increases DNN model generalizability beyond the training by normalizing the distribution of each DNN layer's inputs such that training between upstream and downstream DNN layers converges more efficiently (Ioffe & Szegedy, 2015). Specifically, batch normalization uses the mean and variance of each activation layer with each training mini-batch to normalize the network activation functions so they have a mean of zero and variance of one (Ioffe & Szegedy, 2015). *Variance scaling of initial weights* helps initialize DNN weights and protect against exploding or vanishing gradients; therefore, reducing DNN training time and improving DNN performance (He et al., 2015). It is implemented by determining the variance of output values from each DNN layer and then scaling initial DNN weights such that they share the same distribution (He et al., 2015). *Early stopping* constrains the potential number of training iterations so the optimization process will iteratively check model error from one training step to the next (Goodfellow et al, 2016). This optimization process can be implemented by saving a copy of the model parameters for every DNN training step where model error decreases; when model error does not decrease after a pre-specified number of steps, training is stopped (Goodfellow et al., 2016). Dropout, batch normalization, variance scaling of initial weights, and early stopping can all be implemented using built-in functions in the Keras and TensorFlow libraries. See the Python scripts associated with this study and available on GitHub for further details.

Throughout DNN training, we maintained an input layer of 62 nodes (i.e., one neuron for each feature in Table S1) and one output layer node to represent the regression output of watershed-scale runoff predictions (Table 1). However, to arrive at the final DNN hidden layer architecture, our basic approach was to start with a large number of hidden layers with many nodes and prune both down based on DNN training loss performance (i.e., overall prediction accuracy as well as the time it takes for the DNN to converge to a solution). More specifically, we initialized the DNN architecture with a large number of hidden layers, where the first hidden layer had approximately 10x more nodes than the input layer. Subsequent hidden layers had approximately half as many nodes as the previous hidden layer. Hidden layers 2 and 3 were an exception to this because we observed that slowing down the node "size decay" reduced training loss (i.e., improved DNN predictions). The initial DNN architecture contained 14 hidden layers but we trimmed it down to 7 after monitoring training loss and the DNNs ability (or inability) to converge in a reasonable amount of time. This is one of several suggested approaches for determining DNN hyperparameters such as the number of hidden layers and hidden layer nodes. Beginners may look to established guides that discuss these approaches in more detail (e.g., Nielsen, 2015; Goodfellow et al., 2016; Brownlee, 2018; Chollet & Allaire, 2018; Kim, 2019).

Table 1. Summary of the final deep neural network architecture used to predict monthly watershed-scale runoff for the conterminous United States. Input and hidden layers were initialized using the "he_normal" method and used the PReLU activation function.

Layer	Description	Number of Nodes	Number of Parameters
0	Input	62	N/A
1	Hidden, Dense with Batch Normalization (30% dropout)	1000	68000
2	Hidden, Dense with Batch Normalization (30% dropout)	800	804800
3	Hidden, Dense with Batch Normalization (30% dropout)	600	483600
4	Hidden, Dense with Batch Normalization (30% dropout)	400	242400
5	Hidden, Dense with Batch Normalization (30% dropout)	200	81200
6	Hidden, Dense with Batch Normalization (30% dropout)	100	20600
7	Hidden, Dense with Batch Normalization (30% dropout)	50	5300
8	Output, Dense	1	51

The final DNN developed here consisted of 7 hidden layers with a varying number of neurons per layer: 1000, 800, 600, 400, 200, 100, and 50 neurons for hidden layers 1 to 7, respectively (Table 1). The input layer consisted of 62 nodes (i.e., one for each of the 62 watershed characteristics; Table S1) and the final layer consisted of one node with a linear output given the regression task (i.e., predicting watershed-scale streamflow). For all layers, we initialized weights using the 'he_normal' method (He et al., 2015). For all the hidden layers, we set the dropout rate to 30% and used a Parametric Rectified Linear Unit (PReLU) activation function (He et al., 2015). Additionally, we set the training batch size to 4,096, the number of epochs (i.e., training time steps) to 2,500, and early stopping to 50 time steps. As mentioned previously, we used a 75:25 training:testing split for model development and testing. In model training, we used a Nesterov Adam (i.e., 'nadam') optimizer with mean absolute error (in mm units) as the loss function (Kingma & Ba, 2014; Sutskever et al., 2013). The parameters in Table 1 refer to tunable weights and biases of DNN nodes and edges that are optimized during model fitting. These parameters effectively control non-linear mapping used to relate DNN input and output variables. The number of parameters represents flexibility in this non-linear mapping rather than the dimensionality of the data space. This is in contrast to, for example, linear regression where p variables are used to fit a line passing through each of p points. Best practices such as model evaluation using an independent test sets help reduce the risk of DNN model overfitting.

We used bias (i.e., y-axis intercept), slope, Pearson's correlation coefficient (PCC), and median absolute error expressed as a percentage (MAE) to test DNN performance. We obtained bias, slope, and PCC from the (linear) line-of-best-fit between observed versus modeled watershed-scale runoff. We bootstrapped 95% confidence intervals ($n = 1000$) for MAE and PCC using

SciPy (Virtanen et al., 2019), Pandas (McKinney et al. 2010), and NumPy (van der Walt et al., 2011) Python libraries to determine whether these metrics were statistically meaningful. In addition to determining DNN performance metrics for the test set, we also calculated them for extreme monthly runoff events including those in the test set that were below the 10th percentile (Q10) or above the 90th percentile (Q90). Q10 and Q90 events were calculated from the entire dataset and labeled in the test set. We also calculated DNN performance metrics for non-reference and reference watersheds as well as for each of the nine GAGES-II watershed ecoregions (i.e., Central Plains, East Highlands, Mixed Wood Shield, Northeast, Southeast Coastal Plain, Southeast Plain, West Mountains, West Plains, and West Xeric; Figure S4). In addition to determining overall (i.e., CONUS-scale) DNN testing metrics, we assessed DNN performance at the watershed-scale by calculating the median residual as a percentage for each of the 2,731 watersheds and plotted the result on a CONUS map. We also plotted DNN residuals versus spatio-temporal variables such as time (i.e., month), watershed area, watershed longitude determined at the watershed centroid, and watershed latitude determined at the watershed centroid to evaluate DNN temporal and spatial robustness. For each spatio-temporal variable, we calculated PCC and bootstrapped 95% confidence intervals as discussed above to evaluate whether model residuals lacked robustness.

2.3 Development, Architecture, and Testing of Other Downscaling Approaches

We tested the ability of four other grid-to-watershed-scale conversion approaches to predict observed monthly runoff at the watershed-scale (Table 2). These included: linear ridge regression, SVM, extreme gradient boosting (XGBoost), and ANN modeling approaches. Similar to the DNN, we tested the performance of these four approaches using bias, slope, MAE, and

PCC (*Section 2.2*). The linear ridge regression model used an L1 regularization penalty applied to the loss function (squared error) to impose sparsity on model features (i.e., parameters for variables in Table S1 should not get too large). SVM, described previously (*Section 1*), utilized a linear SVM with L1 regularization (Drucker et al., 1997). XGBoost is a more advanced version of gradient boosting (Friedman; 2001) that incorporates model regularization, parallel processing, and a number of algorithmic innovations that improve model development efficiency and model prediction accuracy (Chen & Guestrin, 2016). Specifically, we used XGBoost to train an ensemble of gradient boosted regressions. The ANN had two hidden layers (Figure S1a). We developed the linear ridge regression, SVM, and XGBoost models via *k*-fold cross-validation coupled with a randomized search process for hyperparameter tuning as described previously by Rice & Emanuel (2017). We used the scikit-learn (version 0.21.2) and XGBoost (version 0.90) Python libraries to train these four models (Pedregosa et al., 2011; Chen & Guestrin, 2016). We used the same computer hardware as described in *Section 2.2*; we trained the ANN and DNN on a GPU and all other models were trained on a CPU.

Table 2. Model performance comparisons relative to observed, monthly runoff at the watershed-scale for the test set. Abbreviations: Generalized Circulation Model (GCM), median absolute error (MAE), Pearson's correlation coefficient (PCC), support vector machine (SVM), extreme gradient boosting (XGBoost), artificial neural network (ANN), deep neural network (DNN), graphics processing unit (GPU), central processing unit (CPU), and not-applicable (N/A). MAE and PCC are reported with the lower and upper 95% confidence intervals in parentheses.

Method	MAE (%)	PCC	Bias (mm)	Slope	Processor	Computing Time (min)
GCM Runoff	49.97 (49.74, 50.2)	0.811 (0.806, 0.815)	6.82	0.85	NA	NA
Monthly Normal Runoff	50.36 (50.10, 50.60)	0.812 (0.809, 0.815)	0.04	1.01	NA	NA
Linear Ridge Regression	>1000	0.155 (0.152, 0.159)	42.68	4.00E-14	CPU	17
SVM	110.11 (109.03, 111.18)	0.772 (0.768, 0.776)	-18.84	1.31	CPU	20
XGBoost	40.28 (40.05, 40.51)	0.933 (0.931, 0.935)	-0.19	1.01	CPU*	300
ANN	35.57 (35.41, 35.73)	0.916 (0.913, 0.917)	-0.29	1.19	GPU	18
DNN	24.31 (24.18, 24.46)	0.962 (0.961, 0.963)	2.36	0.94	GPU	110

* Six cores in parallel

2.4 Comparing Downscaling Approaches

We used three approaches to comparatively assess the predictive power of the five models presented here (i.e., linear ridge regression, SVM, XGBoost, ANN, and DNN). First, we compared observed monthly runoff at the watershed outlet (i.e., the USGS gage) to modeled watershed-scale runoff from the test set. We included comparisons with the test set, with Q10 and Q90 events in the test set, with non-reference and reference watersheds in the test set, and with watersheds in the nine GAGES-II watershed ecoregions in the test set. For these comparisons, we used bias, slope, PCC, and MAE metrics as described in *Section 2.2*. Second, we tested model performance by comparing bias, slope, PCC, and MAE metrics between observed monthly runoff at the watershed outlet and the monthly ensemble of areal averaged GCM runoff (see *Section 2.1* for a full description), which we refer to henceforth as 'GCM runoff'. Third, we assessed model performance by comparing bias, slope, PCC, and MAE metrics between observed monthly runoff and the average of monthly runoff (i.e., observed streamflow at the watershed outlet divided by watershed area) over the 30-year study period, which we refer to henceforth as 'monthly normal runoff'. As with computing GCM runoff, monthly normal runoff was estimated at the watershed extent as described in *Section 2.1*. This process was implemented on a monthly time-step prior to computing 30-year means. We note that monthly normal runoff only relies on three features while the five models mentioned previously rely on 62 features (see Table S1). As a result, GCM runoff and monthly normal runoff serve as model comparison controls.

2.5 Data and Script Availability

We analyzed these data using Python (version 3.7.1, Python Software Foundation, 2018) and R (version 3.4.3; R Core Team, 2017). All model development code, data, trained model weights (i.e., parameters), and scripts associated with this publication are available on GitHub at [insert link here upon manuscript acceptance] and Zenodo (DOI: [insert link here upon manuscript acceptance]).

3 Results

3.1 Deep Neural Network Testing

At the CONUS-scale, the DNN explained 92.5% (PCC = 0.962) of the variation in observed monthly test set runoff ($p < 0.0001$; Figure 2a). Test set DNN residuals were close to zero and roughly symmetric around zero (Figures S5a). DNN MAE was 24.31%, bias was 2.36, and slope was 0.94 for the test set (Table 2). For Q10 events, the DNN explained 77.4% (PCC = 0.880) of variation in observed monthly runoff (Figure 2b). The MAE, bias, and slope were 50.87%, 0.52, and 0.73, respectively for Q10 events (Table S2). For Q90 events, the DNN explained 91.4% (PCC = 0.956) of variation in observed monthly runoff (Figure 2c). The MAE, bias, and slope were equal to 15.96%, 12.94, and 0.94, respectively for Q90 events (Table S2). The DNN explained 91.0% (PCC = 0.954) and 94.3% (PCC = 0.971) of the variation in observed monthly runoff for non-reference and reference watersheds in the test set, respectively (Table S3). The bias of non-reference watersheds in the test set was 2.36 and the slope was 0.94. For the reference watersheds in the test set the bias was 2.60 and the slope was 0.95. When separating out test set results by ecoregion for the DNN, bias ranged from 0.83 to 7.31 (Table S4), slope ranged from 0.87 to 1.08 (Table S5), and PCC ranged from 0.80 to 0.97 (Table S6). DNN residuals were spread around zero when plotted against spatio-temporal variables such as time, latitude, longitude, and watershed area (Figures S5d-S5f, and S6). PCCs between DNN residuals and spatio-temporal variables were close to zero (Figures S5d-S5f, S6, and S10); they ranged from -0.05 to 0.04 (Table 3). At the watershed-scale, DNN median residuals were distributed around zero for test set (Figures 3, S5a, and S7a). The same was true for Q10 and Q90 events (Figures S7b, S7c, S8, and S9). Last, DNN test set median watershed residuals grouped by month were close to zero (Figure S10).

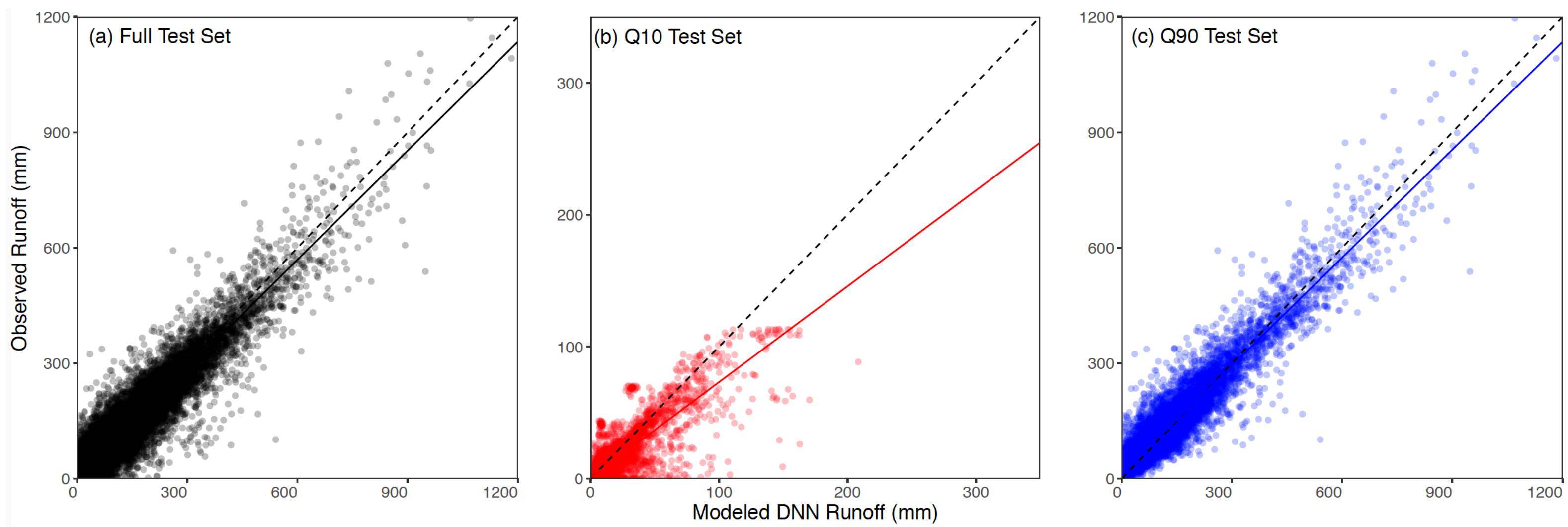

Figure 2. Comparison of deep neural network predicted (a) test set runoff (black, n = 243,376), (b) Q10 test set runoff (red, n = 24,928), and (c) Q90 test set runoff (blue, n = 24,362) versus observed monthly runoff from the GAGES-II dataset. Dashed lines represent 1:1 line and solid lines represent linear regression line-of-best-fit. Note that the x-axis and y-axis scales in (b) are different from (a) and (c).

Table 3. Pearson’s correlation coefficient (PCC), bootstrapped lower 95% confidence intervals (CIs), and bootstrapped upper 95% CIs between DNN residuals and spatio-temporal variables.

Variable	PCC	Lower CI	Upper CI
Time (month)	-0.003	-0.008	0.001
Watershed Area	-0.003	-0.005	-0.001
Latitude	0.040	0.035	0.045
Longitude	-0.050	-0.055	-0.045

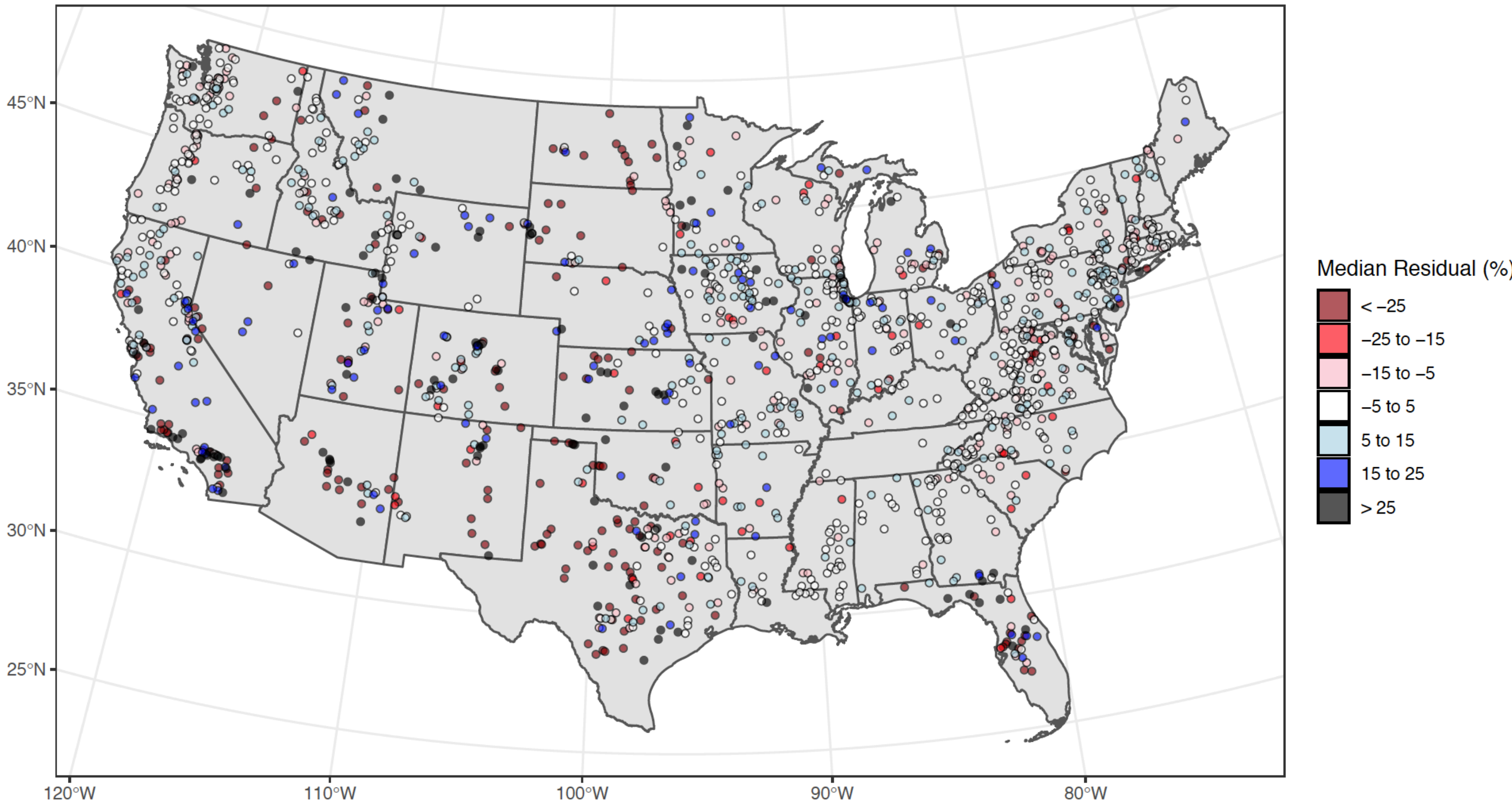

Figure 3. Deep neural network test set median watershed residuals. Point location represents the watershed centroid. Median watershed residuals are expressed as a percent relative to observations.

3.2 Model Performance Comparisons

We included two model controls in this study: GCM runoff and monthly normal runoff. GCM runoff explained 65.8% (PCC = 0.811) and monthly normal runoff explained 65.9% (PCC = 0.812) of the variation in observed monthly test set runoff (Table 2). GCM runoff MAE was 49.97% and monthly normal runoff MAE was 50.36% for the test set. For Q10 events, GCM runoff explained 25.6% (PCC = 0.506) of the variation in observed monthly runoff and had a MAE of 149.05% (Table S2). Monthly normal runoff explained 62.7% (PCC = 0.792) of the variation in observed monthly runoff for Q10 events and had a MAE equal to 293.91% (Table 3). For Q90 events, GCM runoff and monthly normal runoff explained 58.8% (PCC = 0.767) and 75.9% (PCC = 0.871) of variation in observed monthly runoff, respectively (Table S2). GCM runoff MAE was 35.36% and monthly normal runoff was 48.45% for Q90 events; both were lower than the MAE of Q10 events (Table S2). For non-reference watersheds in the test set, GCM runoff and monthly normal runoff had lower PCCs compared to the full test set (Tables 2 and S3). Conversely, for reference watersheds in the test set, GCM runoff and monthly normal runoff had a higher PCC compared to the full test set (Table S3). When looking at test set results by ecoregion, GCM runoff bias ranged from 0.55 to 13.56 (Table S4), slope ranged from 0.56 to 1.07 (Table S5), and PCC ranged from 0.58 to 0.86 (Table S6). For monthly normal runoff test set results analyzed by ecoregion bias ranged from -0.1 to 0.4 (Table S4), slope ranged from 0.99 to 1.03 (Table S5), and PCC ranged from 0.58 to 0.86 (Table S6).

In addition to model controls, we compared DNN performance to four other grid-to-watershed-scale conversion techniques: linear ridge regression, SVM, XGBoost, and ANN (Table 2). Of the four methods, XGBoost explained the most variation in observed monthly test set runoff followed by (in order of decreasing PCC) ANN, SVM, and linear ridge regression techniques (Table 2). For the test set, MAE was smallest for the ANN followed by (in order of increasing MAE) XGBoost, SVM, and linear ridge regression techniques (Table 2). Slopes for the four techniques were all greater than one except for linear ridge regression, which was close to zero (Table 2). For Q10 events, XGBoost explained the most variation in observed monthly test set runoff followed by (in order of decreasing PCC) ANN, SVM, and linear ridge regression techniques (Table S2). MAE was smallest for the ANN followed by (in order of increasing MAE) XGBoost, SVM, and linear ridge regression for Q10 events. Like Q10 events, model results for Q90 events have a similar PCC ranking. XGBoost explained the most variation in monthly observed runoff (Table S2). For Q90 events, MAE was smallest for XGBoost followed by (in order of increasing MAE) ANN, SVM, and linear ridge regression. For non-reference watersheds in the test set, XGBoost followed by (in order of decreasing PCC) ANN, SVM, and linear ridge regression explained the most variation in observed monthly runoff (Table S3).For reference watersheds in the test set, a similar PCC ranking held. When looking at test set results by ecoregion, slopes for the four techniques were typically > 1.0, except for linear ridge regression (Table S5) and PCCs were typically > 0.7 except for in a few cases for SVM and in all cases for linear ridge regression (Table S6).

We assessed model training efficiency by comparing computer processor requirements and computing time. For the DNN and the four alternative grid-to-watershed-scale conversion techniques, the ANN and DNN were the only models requiring a GPU. The DNN took ~ 10 times more computing time than the ANN. Of the techniques using a CPU (i.e., linear ridge regression, SVM, XGBoost), XGBoost took the longest to train; about three times as much time as the DNN. Of all the techniques we tested, linear ridge regression took the least amount of time to train.

4 Discussion

4.1 Deep Neural Network Testing

The trained DNN predicted monthly runoff more accurately than controls (i.e., GCM runoff and monthly normal runoff) and was able to effectively translate gridded GCM outputs into watershed-scale runoff as demonstrated by several key results. First, the DNN explained more variation in observed monthly runoff and had a lower MAE compared to any other methods that we considered (Table 2). Second, the DNN runoff predictions approximated observed runoff with little bias (Figure 2a). Third, DNN residuals were close to zero and were relatively symmetric (Figures S5a, S5b, and S7a). This indicates the absence of a systematic tendency for the DNN to overestimate or underestimate watershed-scale runoff. Fourth, we observed a near-zero correlation between DNN residuals and variables related to time, location, or watershed size (i.e., time, longitude, latitude, and watershed area; Table 3, Figures S5d-S5f, S6, S7, S10). This indicates that the DNN was generally robust to spatio-temporal variation. However, we observed that the DNN overpredicted monthly runoff in California, Texas, and Florida as indicated by large negative (i.e., < -25%) median watershed residuals (Figure 3). Future studies may use local interpretable model-agnostic explanations (LIME; Ribeiro et al., 2018) and other machine learning interpretation techniques to further explain these patterns in model residuals (e.g., Worland et al., 2019).

The trained DNN adequately predicted monthly Q10 and Q90 runoff events, although, Q90 events tended to be more accurately predicted than Q10 events. More specifically, the DNN explained a larger percentage of variation (i.e., higher PCC) in observed monthly runoff test set Q90 events compared to Q10 events (Table S2). Also, the scatter plot of observed versus modeled runoff for Q90 events tracked the 1:1 line closer than that for Q10 events (Figures 2b and 2c). Points below the 1:1 line support the finding that the DNN tended to overpredict Q10 events (Figure 2b). We also observed a higher MAE for Q10 events compared to Q90 events (Table S2). Compared to GCM runoff and monthly normal runoff, the DNN was more effective at predicting Q10 and Q90 monthly runoff events as supported by a consistently higher PCC and lower MAE.

In addition to scale (i.e., CONUS- and watershed-scale) and extreme events, the DNN accurately predicted monthly runoff for non-reference as well as reference watersheds and across all nine GAGES-II watershed ecoregions. More specifically, PCC for non-reference watersheds in the test set was 0.954 and 0.971 for reference watersheds in the test set (Table S3). Bias was less than 8, slope was close to one, and PCC was > 0.8 for watersheds in all ecoregions. We observed the largest PCC in the West Mountains (Table S6). Compared to GCM runoff and monthly normal runoff, the DNN was better at predicting non-reference and reference site monthly runoff as supported by a consistently higher PCC and lower MAE (Table S3).

4.2 Model Performance Comparisons

Compared to the four other grid-to-watershed-scale conversion techniques, the DNN explained the most variation in observed monthly runoff (i.e., highest PCC) and had the lowest MAE (Table 2). We found that linear ridge regression and SVM methods all had higher MAE, higher bias (either negative or positive), and lower PCC than the control methods (i.e., GCM runoff and monthly normal runoff; Table 2). Therefore, we do not recommend using these methods for converting gridded, downscaled monthly GCM hydroclimatic fluxes to watershed-scale monthly runoff for the CONUS. The ANN, which represents a simpler neural network structure compared to the DNN (Figure S1a), could adequately predict monthly runoff, albeit not as well as the DNN (Table 2). This finding is likely explained by the difference in hidden layers between the ANN and DNN. The DNN has more hidden layers, which enable it to represent more complex relationships between data inputs and outputs (Shen, 2018). XGBoost predicted monthly runoff better than controls, had a higher PCC and MAE than the ANN, but underperformed relative to the DNN (Table 2).

The DNN outperformed the model controls as well as the four alternative techniques when it came to predicting Q10 and Q90 monthly runoff, non-reference and reference monthly runoff, and monthly runoff in various ecoregions. Similar to the results discussed above, we do not recommend the linear ridge regression because this technique tended to perform worse than model controls for Q10 and Q90 events; it had a higher MAE and lower PCC (Table S2). Linear ridge regression also had a lower PCC than the controls for non-reference and reference watersheds (Table S3) as well as for watersheds in all ecoregions (Table S6). SVM sometimes outperformed the model controls for Q10 and Q90 events, but there were some exceptions to this finding (e.g., the MAE for Q10 events was 736%; Table S2). SVM tended to have a lower PCC compared to the model controls for non-reference and reference watersheds (Table S3) as well as for watersheds in some ecoregions (e.g., West Mountains). While not as accurate as the DNN, XGBoost and ANN consistently had a lower MAE and higher PCC for Q10 and Q90 monthly runoff compared to model controls (Table S2). Additionally, compare to model controls, XGBoost and ANN had a higher PCC for non-reference and reference watersheds as well as watersheds in all ecoregions.

When it came to computing power, we found that the DNN required the second longest computing time and a GPU compared to all the other grid-to-watershed-scale monthly runoff conversion methods tested (Table 2). However, other well performing approaches required either a GPU (i.e., ANN) or parallel computing on a CPU (i.e., XGBoost; Table 2). This finding highlights a potential limitation of DNN-based methods; hydrologists interested in using machine learning methods to convert gridded GCM hydroclimatic fluxes to watershed-scale runoff may wish to consider available computing resources before implementing DNNs. DNNs can be trained on a single desktop workstation in less than a day using open-source software or users may seek out cloud-based computing methods to carry out analyses if research budgets are more limited. Based on these results, DNNs hold great promise as a tool for improving the accuracy of GCM-derived runoff estimates for watershed-scale research.

4.3 Applying Deep Learning to Climate Model Downscaling: Examples in Colorado and North Carolina, USA

To illustrate the efficacy of using the DNN to convert gridded, downscaled GCM outputs to watershed-scale runoff, we consider two example watersheds (Figure 4a). USGS stream gage number 09163500 measures runoff for the portion of the Colorado River that flows through Colorado, USA (henceforth referred to as the Upper Colorado River Watershed; UCR) and USGS stream gage number 02129000 measures runoff for the Yadkin-Pee Dee River Watershed (YPD). The UCR an area of 46,300 km^2 and the YPD has an area of 17,800 km^2. Both are characterized as non-reference (i.e., human-disturbed) watersheds (Falcone et al., 2010).

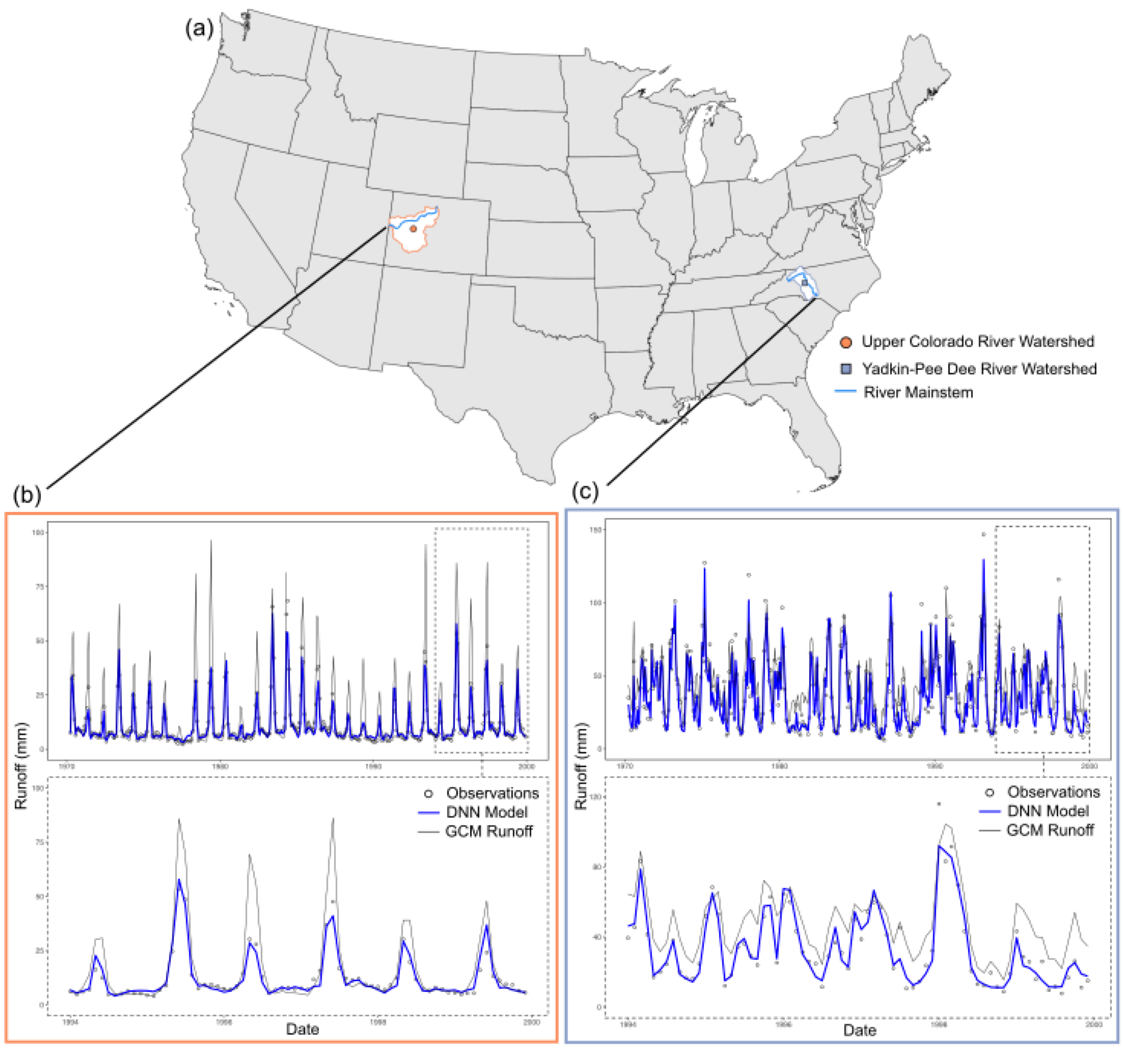

Figure 4. Examples of the Upper Colorado River Watershed (UCR) in the Southwest United States and Yadkin-Pee Dee River Watershed (YPD) in the Southeast United States. (a) Location of UCR centroid (orange circle) and boundary and YPD centroid (blue square) and boundary. (b) Comparison of UCR observed runoff (empty circles), DNN modeled runoff (thick blue solid line), and GCM runoff (thin black solid line) versus time. (c) Comparison of the same results for the YPD. Bottom plot of (b) and (c) includes the five most recent years of the time series.

In 2006, the UCR consisted of primarily (53.8%) forest land cover, followed by 24% shrubland, 9.9% grassland, 4.1% agriculture, 3.8% barren, 1.7% wetlands, and 1.5% development, and 1.1% water (including snow and ice; Falcone et al., 2010; Fry et al., 2012). While the fraction of development within the watershed is low, it is a key water source for ecosystems and downstream residents in the southwestern US (McCabe & Wolock, 2007; Udall & Overpeck, 2017). Climate change is projected to increase temperatures by 2-4°C in the Southwest United States by 2050, leading to decreases in snowpack, increases in drought duration, and decreases in runoff (Seager & Vecchi, 2010; Hayhoe et al., 2018; Gonzalez et al., 2018). Consequently, climate change will likely stress regional water supplies that are already very sensitive to changes in runoff (McCabe & Wolock, 2007; Christensen & Lettenmaier, 2006; Woodhouse et al., 2016, Udall & Overpeck 2017).

Given these sensitives in water resources management to changes in UCR runoff, it is important to accurately downscale GCM results to the watershed-scale. Compared to observations, GCM runoff predictions for the UCR had a MAE of 25.2%. Using the DNN developed by this study, the MAE of monthly runoff for the UCR was 12.2%; nearly 50 percentage points better. More specifically, many of the monthly runoff peaks were overpredicted by GCM runoff (Figure 4b). To put these numbers into perspective, mean monthly runoff from this basin during the study period was 11.0 mm, or 511 million m^3. Using that value as a guideline, the reduction in error associated with applying the correction model to monthly, gridded GCM runoff for the UCR equates to an improvement in accuracy on the order of 66 million m^3 of water per month (i.e., 511 million m^3 x 0.252 minus 511 million m^3 x 0.122), which is 2.8-5.6% of the total monthly water withdrawals for Colorado in 2015 (Dieter et al., 2018). For the UCR, the DNN enhanced the accuracy of GCM runoff and GCM output applicability to water resources management.

In 2006, the YPD consisted of mainly (53.8%) forest land cover, followed by 24.8% agriculture, 12.5% developed, 4.8% grassland, 1.8% shrubland, 1.3% water, 1% wetlands, and <1% barren lands (Falcon et al., 2010; Fry et al., 2012). Compared to UCR, the YPD has more development which is projected to increase 101-192% in the Southeast United States by 2060 (Terando et al., 2014). This development will largely replace forested land cover (USFS, 2012; Wear, 2013). Climate change is projected to increase regional temperatures 2.2-2.6°C by 2100 and future precipitation is likely to be more extreme, including more intense events and longer periods between events (O'Gorman & Schneider 2009; Laseter & others 2012; IPCC 2014; Walsh et al. 2014; Carter et al. 2018). In the YPD, these land cover and climate changes may combine to increase peak flows and reduce groundwater recharge (Ogden et al., 2011; Hamel et al., 2013; Walsh et al., 2014; Martin et al., 2017; Carter et al., 2018; Suttles et al., 2018). This increase number of future high flow events may negatively impact vulnerable communities in the YPD (Saia et al., 2019).

Compared to observations, GCM runoff predictions for the YPD had a MAE of 46.1%. Using the DNN developed by this study, the MAE of monthly runoff for the YPD was 9.58%; nearly 80 percentage points better. Unlike the UCR where monthly runoff peaks were overpredicted, GCM runoff seemed to overpredict peaks as well as time points between peaks for the YPD (Figure 4c). Mean monthly runoff from this basin during the study period was 36.4 mm, or 647 million m^3. Using that value as a guideline, the reduction in error associated with applying the correction model to monthly, gridded GCM runoff for the UCR equates to an improvement in accuracy on the order of 236 million m^3 of water per month (i.e., 647 million m^3 x 0.461 minus 647 million m^3 x 0.0958), which is about 10-20% of the total monthly water withdrawals for North Carolina in 2015 (Dieter et al., 2018). Many studies conducted in and around YPD region (e.g., Martin et al., 2018 and Suttles et al., 2018) note the importance of managing forest land cover in the face of projected climate and land use change. More accurate runoff predictions may improve forest land cover management, and ultimately, water resources (Vose, 2018).

4.4 Implications and Future Directions

To the best of our knowledge, this study was the first to combine watershed characteristics from a large publicly available dataset with gridded GCM hydroclimatic fluxes (i.e., precipitation, temperature, and evapotranspiration) to develop a DNN that accurately predicted monthly runoff for watersheds across the CONUS (Figure S2). The trained DNN was robust to spatio-temporal changes in monthly runoff, accounted for non-reference and reference site characteristics, and was robust across the nine GAGES-II watershed ecoregions. Additionally, the trained DNN adequately predict Q90 events; however, it had a more difficult time predicting Q10 events. We also compared DNN runoff predictions to two controls (i.e., GCM runoff and monthly normal runoff) and four statistical grid-to-watershed-scale conversion techniques. The DNN outperformed all alternative techniques but required more computing power and computing time than some alternatives. This work highlights key benefits of DNNs as well as future opportunities for the application of DNNs to statistical GCM downscaling.

In addition to key benefits discussed in *Section 1*, DNN structure—including input, hidden, and output layers (Figure S1b)—conserves the conceptualization of watersheds as spatio-temporal filters (e.g., Weiler et al., 2003; Nippgen et al., 2011; Emanuel et al., 2014; Rice et al., 2015; Rice & Emanuel, 2019). The concept underpins the Geomorphic Instantaneous Unit Hydrograph (GIUH; Rodriguez-Iturbe & Valdes, 1979; Gupta et al., 1980; Rinaldo et al., 1995; Nippgen et al., 2015) and hydrologic similarity (Beven & Kirkby, 1979; Brutsaert, 1994; Lyon & Troch, 2007). In the context of this study, watersheds translate hydroclimatic input signals into runoff output signals given interaction between internal watershed characteristics (e.g., soil saturation) that occurs in the context of external hydroclimatic inputs. As an example, geomorphic and topographic landscape structures (Emanuel et al., 2010; Jencso & McGlynn, 2011; Nippgen et al., 2011) and patterns in vegetation and land cover (Rodriguez-Iturbe, 2000; DeFries & Eshlemann, 2004; Piao et al., 2007; Emanuel et al., 2010; 2014; Nippgen et al., 2015) control the movement of water through watersheds. Although hidden layers may or may not represent recognizable hydrologic processes, the DNN effectively learns a representation of the overarching conceptualization of watersheds as filters from the data.

Using DNNs to represent watershed signal filtering is also consistent with current understanding of watersheds as complex systems comprising non-linear feedbacks and other interactions (McDonnell et al., 2007). We suggest that DNNs can account for non-linear interactions between spatial biotic, abiotic, endogenous, and exogenous features that yield watershed-scale memory effects, and ultimately, result in emergent streamflow responses (Nippgen et al., 2016) and land-atmosphere biogeochemical fluxes (Emanuel et al., 2011; Riveros-Iregui et al., 2012; Reyes et al., 2017). Existing governing equations may represent some of these behaviors, but machine learning models such as DNNs have the ability to independently uncover previously unrecognized or unparameterized feedbacks contained within large datasets publicly available to hydrologists. When adequate training data and training time are available, DNNs serve as universal function approximators (LeCun et al., 2015; Goodfellow et al., 2016; Rolnick & Tegmark, 2017; Knighton et al., 2019); where in the case of watershed-scale runoff prediction, the universal function likely describes some of these non-linear feedbacks occurring within the watershed. A deeper look at these universal functions may confirm or challenge aspects of our existing conceptual understanding of watersheds and runoff processes. Thus, probing of DNN results may help hydrologists (1) develop hypotheses concerning understudied or unidentified interactions between hydroclimatic fluxes, watershed characteristics, and runoff and (2) test these hypotheses using physically-based modeling and field studies (Shen et al., 2018).

While this study does not attempt to characterize the filtering processes of watersheds across the CONUS, future studies may apply tools such as partial response functions (Rice et al., 2016; Rice & Emanuel, 2017) and local interpretable model-agnostic explanations (Worland et al., 2019) to explore the impact of GCM inputs and watershed characteristics on watershed-scale runoff. Also, these statistical model interpretation methods may be used to open up the machine learning "black box" by generating hypotheses that can be tested using physically-based hydrology models and field experiments (Shen et al., 2018; Rice and Emanuel 2019). For example, one study combined XGBoost results with the Budyko framework (Budyko, 1974) to assess the impact of forest land cover on watershed storage (Rice & Emanuel, 2019). Another study used gridded GCM climate variables to develop a convolutional neural network—a specific type of DNNs that relies on 2D inputs such as images—and then to interpret seasonal extreme precipitation patterns in the Eastern United States using archetypal analysis (Knighton et al., 2019). We incorporated methods to improve model training and testing when it comes to temporal changes in runoff (i.e., semi-random sampling and residual trend analysis); however, additional opportunities exist to train and test DNN model response to non-stationary processes. This may include the use of covariate shift adaptation (Sugiyama et al., 2007) in hydrological science machine learning applications and long short-term memory (LSTM) neural networks (Shen, 2018).

4.5 Recommendations for DNN Applications in the Hydrologic Sciences

With the growing emergence of big data and machine learning methods, this study serves as a guide to hydrologists interested in implementing machine learning techniques such as DNNs. In this study we applied a DNN to convert GCM runoff to the watershed-scale but DNNs could be used more broadly to convert other gridded data products (e.g., Gravity Recovery and Climate Experiment; GRACE, Moderate Resolution Imaging Spectroradiometer-Evapotranspiration; MODIS-ET, Coupled Model Intercomparison Project Phase 6; CMIP6) to the watershed-scale. Below we note a few practical experimental design considerations for hydrologic scientists and researchers; however, we also suggest recent publications by Shen (2018), Shen et al. (2018), and Worland et al. (2019) for didactic texts on deep neural network applications in hydrology.

- *training and test splits* - Similar to standards methods for hydrology model evaluation (i.e., Moriasi et al., 2007), researchers designing DNN-based experiments should separate full datasets up into a train and test sets. Typical splits are 75:25 (75% training and 25% testing) or 80:20, but the exact split is less important as ensuring the creation of an independent test set to evaluate model performance. As in other types of model training, DNN training uses only the train set and is evaluated based on the independent test set, which it has never "seen". Ideally, the DNN may also be evaluated based a separate validation set that includes newly generated data. For example, this may include using current precipitation and temperature data as inputs to the model. Researchers may also wish to consider their method for splitting up data (i.e., random sampling or semi-random hold out). Here, we used semi-random sampling because we wanted to make sure the DNN was robust in time and space. Thus, we are choosing which input variables are important for the DNN to represent.

- *model evaluation metrics* - Consider using multiple model evaluation metrics when assessing DNN performance. These may include bias, slope, R^2, and MAE as well as others we do not use here (e.g., Nash- Sutcliffe Efficiency). For a thorough review of standard hydrology model evaluation metrics see Moriasi et al. (2007).
- *residual analysis* - Residual analysis including the plotting of residuals versus observations, and in this case, important spatio-temporal variables is an important statistical evaluation technique to assessing whether or not the DNN is robust to changes in model inputs.
- *architecture* - Researchers should consider whether they will start simply and add layers and nodes or start with a large model and remove layers and nodes. Both approaches can lead to useful capabilities, as we discussed in *Section 2.2*.
- *model training improvement techniques* - In this study, we implemented a number of techniques to improve model training accuracy and reduce model training time (e.g., early stopping). Researchers should consider including some of these; fortunately, many

are easily implemented using existing Python and R libraries. For a thorough description of these techniques, look to Goodfellow et al. (2016).

- *data quality and research framing* - The old adage "garbage in, garbage out" is important to consider when it comes to implementing machine learning methods. If your data are biased, the machine learning model may learn to reproduce those biases. For example, if a DNN model is conditioned only on water samples collected after a precipitation event, the model may have a hard time predicting water quality metrics before or during a storm. Just as importantly, it is key to be mindful that machine learning, while powerful, is simply another tool for extracting insights from data. Therefore, machine learning is best used in combination with well-framed research questions and relevant, high quality data.

5 Conclusions

We used a large publicly available dataset from the United States Geological Survey combined with monthly, gridded, downscaled, general circulation model (GCM) hydroclimatic fluxes (i.e., precipitation, evapotranspiration, and temperature) to train and test a deep neural network (DNN) capable of predicting monthly runoff at the watershed-scale for 2,731 watersheds across the conterminous United States. We also compared DNN performance to the performance of four other grid-to-watershed-scale conversion techniques, including: linear ridge regression, support vector machine, extreme gradient boosting, and an artificial neural network. Of all these modeling approaches, the DNN had the lowest median absolute error, the lowest bias, and explained the most variation in observed monthly runoff. Furthermore, the DNN was temporally and spatially robust and represented extreme low (i.e., monthly runoff events in the 10^{th}

percentile or lower; Q10) and extreme high (i.e., monthly runoff events in the 90th percentile or higher; Q90) relatively well compared to the four other grid-to-watershed-scale conversion techniques. However, of all the approaches we tested, the DNN took the second longest to train using specialized computing hardware (i.e., a graphical processing unit; GPU). Finally, we presented example results in the Upper Colorado River Watershed and Yadkin-Pee Dee River Watershed to demonstrate how the DNN improved upon raw, gridded GCM runoff data and why this improvement is relevant for water resources management in these regions. Overall, this study highlights the emerging role of machine learning techniques such as DNNs for hydrologic and environmental science research.

Acknowledgements

Author Contributions: JSR and REE designed the study. SMS and JSR analyzed the data. All authors interpreted the data. SMS and JSR drafted the manuscript. SMS and JSR prepared data and code for GitHub/Zenodo. All authors provided critical revision.

This work is supported by the National Science Foundation (Grant Number: EAR 1558675) and by the Department of Forestry and Environmental Resources at North Carolina State University. All model development code, data, trained model weights (i.e., parameters), and scripts associated with this publication are available on GitHub at [insert link here upon manuscript acceptance] and Zenodo (DOI: [insert link here upon manuscript acceptance]).

References

Abadi, M., Agarwal, A., Barham, P., Brevdo, E., Chen, Z., et al. (2015). TensorFlow: Large-scale machine learning on heterogeneous systems. Available online: https://www.tensorflow.org/.

Alkama, R., Marchand, L., Ribes, A., & Decharme, B. (2013). Detection of global runoff changes: results from observations and CMIP5 experiments. *Hydrology and Earth Systems Sciences*, 17, 2967-2979.

Arritt, R. W., & Rummukainen, M. (2011). Challenges in regional-scale climate modeling. *Bulletin of the American Meteorological Society*, 92, 365-368.

Baker, I. T., Sellers, P. J., Denning, A. S., Medina, I., Kraus, P., Haynes, K. D., & Biraud, S. C. (2017). Closing the scale gap between land surface parameterizations and GCMs with a new scheme, SiB3-Bins. *Journal of Advances in Modeling Earth Systems*, 9, 691-711.

Beven, K. J., & Kirkby, M. J. (1979). A physically based, variable contributing area model of basin hydrology. *Hydrological Sciences Bulletin*, 24, 43-69.

Blöschl, G., Bierkens, M. F. P., Chambel, A., Cudennec, C., Destouni, G., et al. (2019). Twenty-three Unsolved Problems in Hydrology (UPH) – a community perspective. *Hydrological Sciences Journal*, 10, 2150-3435.

Bonan, G. B. (1997). Effects of land use on the climate of the United States. *Climatic Change*, 37, 449-486.

Bring, A., Asokan, S. M., Jaramillo, F., Jarsio, J., Levi, L., Pietron, J., Prieto, C., Rogberg, P., & Destouni, G. (2015). Implications of freshwater flux data from the CMIP5 multimodel output across a set of Northern Hemisphere drainage basins. *Earth's Future*, 3, 206-217

Brownlee, J. (2018). *Better Deep Learning: Train Faster, Reduce Overfitting, and Make Better Predictions*, eBook Edition 1.4, Machine Learning Mastery, Victoria, Australia, 539p.

Brutsaert, W. (1994). The unit response of groundwater outflow from a hillslope. *Water Resources Research*, 30, 2759-2763.

Budyko, M. I. (1974). *Climate and life*. New York, NY: Academic Press.

Carter, L. A., Terando, A., Dow, K., Hiers, K. Kunkel, K. E., Lascurain, A., et al. (2018). *Chapter 19: Southeast. Impacts, Risks, and Adaptation in the United States: Fourth National Climate Assessment*. (eds) D. R. Reidmiller, C. W. Avery, D. R. Easterling, K. E. Kunkel, K. L. M. Lewis, T. K. Maycock, & B. C. Stewart. U.S. Global Change Research Program, Washington, DC. p743-808.

Cavazos, T. (2000). Using Self-Organizing Maps to Investigate Extreme Climate Events: An Application to Wintertime Precipitation in the Balkans. *Journal of Climate*, 13, 1718-1732.

Charles, S. P., Bates, B. C., Smith, I. N., & Hughes, J. P. (2004). Statistical downscaling of daily precipitation from observed and modelled atmospheric fields. *Hydrological Processes*, 18, 1373-1394.

Chen, T., & Guestrin, C. (2016). XGBoost: A Scalable Tree Boosting System. *KDD 2016 Proceedings of the 22nd ACM SIGKDD International Conference on Knowledge Discovery and Data Mining*, 785-794. Available online: https://dl.acm.org/citation.cfm?doid=2939672.2939785

Chen, J., Theller, L., Gitau, M. W., Engle, B. A., & Harbor, J. M. (2017). Urbanization impacts on surface runoff of the contiguous United States. *Journal of Environmental Management*, 187, 470-481.

Chiew, F. H. S., Teng, J., Post, D. A., Perraud, J. M., Kirono, D. G. C., & Viney, N. R. (2009). Estimating climate change impacts on runoff across southeast Australia: Method, results, and implications of the modeling method. *Water Resources Research*, 45, W10414.

Chollet, F., et al. (2015). Keras library documentation. Available online: https://github.com/fchollet/keras.

Chollet, F., & Allaire, J. M. (2018). *Deep Learning with R*. 1st Edition, Manning Publications Co, Greenwich, CT, USA.

Christensen, N., & Lettenmaier, D. (2006). A multimodel ensemble approach to assessment of climate change impacts on the hydrology and water resources of the Colorado River basin. *Hydrology and Earth Systems Sciences Discussions*, 3, 3727-3770.

Dawson, C. W., & Wilby, R. (1998). An artificial neural network approach to rainfall-runoff modelling. Hydrological Sciences Journal, 43, 47-66.

DeFries, R., & Eshleman, K. N. (2004). Land-use change and hydrologic processes: a major focus for the future. *Hydrological Processes*, 18, 2183-2186.

Dieter, C. A., Maupin, M. A., Caldwell, R. R., Harris, M. A., Ivahnenko, T. I., Lovelace, J. K., et al. (2018). *Estimated use of water in the United States in 2015*: U.S. Geological Survey Circular 1441, 65 p., Available online: https://doi.org/10.3133/cir1441. [Supersedes USGS Open-File Report 2017–1131.]

Drucker, H., Burges, C. J. C., Kaufman, L., Smola, A., & Vapnik, V. (1997). *Support vector regression machines, in Advances in Neural Information Processing Systems*. MIT Press, Cambridge, MA. p155-161.

Dynesius, M., & Nilsson, C. (1994). Fragmentation and flow regulation of river systems in the northern third of the world. *Science*, 266, 753-762.

Emanuel, R. E., Epstein, H. E., McGlynn, B. L., Welsch, D. L., Muth, D. J., & D'Odorico, P. (2010). Spatial and temporal controls on watershed ecohydrology in the northern Rocky Mountains. *Water Resources Research*, 46, W11553.

Emanuel, R. E., Hazen, A. G., McGlynn, B. L., & Jencso, K. G. (2014). Vegetation and topographic influences on the connectivity of shallow groundwater between hillslopes and streams. *Ecohydrology*, *7*, 887-895.

Emanuel, R. E., Riveros-Iregui, D. A., McGlynn, B. L., & Epstein, H. E. (2011). On the spatial heterogeneity of net ecosystem productivity in complex landscapes. *Ecosphere*, 2, 86.

Emanuel, R. E., Buckley, J. J., Caldwell, P. V., McNulty, S. G., & Sun, G. (2015). Influence of basin characteristics on the effectiveness and downstream reach of interbasin water transfers: displacing a problem. *Environmental Research Letters*, 10, 124005.

Environmental Systems Research Institute (ESRI). (2011). ArcGIS desktop, version 10.4.1.

European Network for Earth Systems (ENES). (2016). *CMIP5 Models and Grid Resolutions*. Accessed 23 Aug. 2016, Available online: https://portal.enes.org/data/enes-model-data/cmip5/resolution.

Falcone, J. A., Carlisle, D. M., Wolock, D. M., & Meador, M. R. (2010). GAGES: A stream gage database for evaluating natural and altered flow conditions in the conterminous United States. *Ecology*, 91, 621-621.

Fowler, H. J., Blenkinsop, S., & Tebaldi, C. (2007). Linking climate change modelling to impacts studies: recent advances in downscaling techniques for hydrological modelling. *International Journal of Climatology*, *27*, 1547-1578.

Friedman, J. H. (2001). Greedy function approximation: A gradient boosting machine. *The Annals of Statistics*, 29, 1189-1232.

Ghosh, S., & Mujumdar, P. P. (2008). Statistical downscaling of GCM simulations to streamflow using relevance vector machines. *Advances of Water Resources*, 31, 132-146.

Glorot, X., & Bengio, Y. (2010). Understanding the difficulty of training deep feedforward neural networks. *Proceedings of the 13th International Conference on Artificial Intelligence and Statistics*, 9, JMLR, Sardinia, Italy.

Gonzalez, P., Garfin, G. M., Breshears, D. D., Brooks, K.M., Brown, H.E., Elias, E.H. et al. (2018). *Chapter 25: Southwest. In Impacts, Risks, and Adaptation in the United States*: Fourth National Climate Assessment, Volume II, (eds.s) Reidmiller, D. R., Avery, C.W., Easterling, D.R., Kunkel, K.E., Lewis, K.L.M., Maycock, T.K., and Stewart, B.C. U.S. Global Change Research Program, Washington, DC, USA, pp. 1101–1184.

Goodfellow, I., Bengio, Y., & Courville, A. (2016). *Deep Learning*, MIT Press, Cambridge, MA. Available online: http://www.deeplearningbook.org/.

Guo, J., Xiong, W., & Chen, H. (2009). Application of Relevance Vector Machine to Downscale GCMs to Runoff in Hydrology. *Sixth International Conference on Fuzzy Systems and Knowledge Discovery*, IEEE Computer Society, 177-182.

Gupta, V. K., Waymire, E., & Wang, C. T. (1980). A representation of an instantaneous unit hydrograph from geomorphology. *Water Resources Research*, *16*, 855-862.

Hamel, P., Daly, E. & Fletcher, T. D. (2013). Source-control stormwater management for mitigating the impacts of urbanisation on baseflow: A review. *Journal of Hydrology*, 485, 201–11.

Hayhoe, K., Wuebbles, D. J., Easterling, D. R., Fahey, D. W., Doherty, S., Kossin, J., et al. (2018). *Chapter 2: Our Changing Climate. Impacts, Risks, and Adaptation in the United States*, Fourth National Climate Assessment, (eds.) DR Reidmiller, CW Avery, DR Easterling, KE Kunkel, KLM Lewis, TK Maycock, and BC Stewart. United States Global Research Program, Washington, DC. p72–144.

He, K., Zhang, X., Ren, S., & Sun, J. (2015, preprint). Delving deep into rectifiers: Surpassing human-level performance on ImageNet classification. Available online: https://arxiv.org/abs/1502.01852.

Hewitson, B. C., & Crane, R. G. (1996). Climate downscaling: techniques and application. *Climate Research*, 7, 85-95.

Hsiang, S., Burke, M., & Miguel, E. (2013). Quantifying the Influence of Climate on Human Conflict. *Science*, 341, 6151.

Hsiang, S., Kopp, R., Jina, A., Rising, J., Delgado, M., et al. (2017). *Science*, 356, 1362-1369.

Hwang, T., Band, L., & Hales, T. C. (2009). Ecosystem processes at the watershed scale: Extending optimality theory from plot to catchment. *Water Resources Research*, 45, W11425.

Ioffe, S., & Szegedy, C. (2015, preprint). Batch normalization: Accelerating deep network training by reducing internal covariate shift. Available online: https://arxiv.org/abs/1502.03167.

Intergovernmental Panel on Climate Change (IPCC). (2007a). *Climate Change 2007: The Physical Science Basis, Contribution of Working Group I to the Fourth Assesment Report of the IPCC (AR4)*. S. Soloman, D. Qin, M. Manning, Z. Chen, M. Marquis, B. Averyt, M. Tignor, & H. L. Millers (eds). Cambridge University Press, Cambridge, U.K.

Intergovernmental Panel on Climate Change (IPCC). (2007b). *Impacts, Adaptation, and Vulnerability, Contribution of Working Group II to the Fourth Asessment Report of the IPCC*

(AR4). M. L. Parry, O. F. Canziani, J. P. Palutikof, P. J. van der Linden, & C. E. Hanson (eds). Cambridge University Press, Cambridge, U.K.

International Panel on Climate Change (IPCC). (2014). *Climate Change 2014: Synthesis Report. Contribution of Working Groups I, II and III to the Fifth Assessment Report of the Intergovernmental Panel on Climate Change*. (eds.) Core Writing Team, RK Pachauri, LA Meyer. IPCC, Geneva, Switzerland. 151p.

Jencso, K. G., & McGlynn, B. L. (2011). Hierarchical controls on runoff generation: Topographically driven hydrologic connectivity, geology, and vegetation. *Water Resources Research*, 47, W11527.

Kim, S. (2019). The Incomplete Deep Learning Guide. Available online at: https://github.com/sannykim/deep-learning-guide.

Kingma, D., & Ba, J. (2014, preprint). Adam: A Method for Stochastic Optimization. Available online: https://arxiv.org/abs/1412.6980.

Knighton, J., Pleiss, G., Carter, E., Lyon, S., Walter, M. T., & Steinschneider, S. (2019). Potential Predictability of Regional Precipitation and Discharge Extremes Using Synoptic-Scale Climate Information via Machine Learning: An Evaluation for the Eastern Continental United States. Journal of Hydrometeorology, 20, 883-900.

Kummu, M., Ward, P. J., de Moel, H., & Varis, O. (2010). Is physical water scarcity a new problem? Global assessment of water shortage over the last two millennia. *Environmental Research Letters*, 5, 034006.

Kunkel, K. E., Stevens, L. E., Stevens, S. E., & Sun, L. (2013). *Regional Climate Trends and Scenarios for the U.S. National Climate Assessment. Part 2. Climate of the Southeast U.S.* NOAA Technical Report NESDIS 142-2, Washington, DC, 103p.

Laseter, S. H., Ford, C. R., Vose, J. M., & Swift, L. W. (2012). Long-term temperature and precipitation trends at the Coweeta Hydrologic Laboratory, Otto, North Carolina, USA. *Hydrology Research*, 43, 890-901.

LeCun, Y., Bengio, Y., & Hinton, G. (2015). Deep Learning, *Nature*, 521, 436-444.

Lyon, S. W., & Troch, P. A. (2007). Hillslope subsurface flow similarity: Real-world tests of the hillslope Peclet number. *Water Resources Research*, 43, W07450.

Manson, S. M. (2001). Simplifying complexity: a review of complexity theory. *Geoforum*, 32, 405-414.

Martin, K. L., Hwang, T., Vose, J. M., Coulston, J. W., Wear, D. N., Miles, B., & Band, L. E. (2017). Watershed impacts of climate and land use changes depend on magnitude and land use context. *Ecohydrology*, 10, 1–17.

Maurer, E. P., Brekke, L., Pruitt, T., & Duffy, P. B. (2007). Fine-resolution projections enhance regional climate change impact studies, *Eos Transactions, American Geophysical Union*, 88, 504.

McCabe, G. J., & Wolock, D. M. (2007). Warming may create substantial water supply shortages in the Colorado River basin. *Geophysical Research Letters*, 34, L22708.

McDonnell, J. J., Sivapalan, M., Vaché, K., Dunn, S., Grant, G., et al. (2007). Moving beyond heterogeneity and process complexity: A new vision for watershed hydrology. *Water Resources Research*, 43, W07301.

McKinney, W. (2010). Data Structures for Statistical Computing in Python, Proceedings of the 9th Python in Science Conference, 51-56. (publisher link)

Milly, P. C. D., Wetherald, R. T., Dunne, K. A., & Delworth, T. L. (2002). Increasing risk of great floods in a changing climate, *Nature*, 415, 514-517.

Milly, P. C. D., Betancourt, J., Falkenmark, M., Hirsch, R. M., Kundzewicz, Z. W., Lettenmaier, D. P., & Stouffer, R. J. (2008). Stationarity is dead: Whither water management?. *Science*, 319, 573-574.

Moriasi, D. N., Arnold, J. G., Van Liew, M. W., Bingner, R. L., Harmel, R. D., Veith, T. L. (2007). Model evaluation guidelines for systematic quantification of accuracy in watershed simulations. Trans. *American Society of Agricultural and Biological Engineers*, 50(3), 885–900.

Moss, R. A., Edmonds, J. A., Hibbard, K. A., Manning, M. R., Rose, S. K., et al. (2010). The next generation of scenarios for climate change research and assessment, *Nature*, 463, 747-756.

Munoz, S. E., Giosan, L., Therrell, M. D., Remo, J. W. F., Shen, Z., et al. (2018). Climatic control of Mississippi River flood hazard amplified by river engineering. *Nature*, 556, 95-98.

National Research Council (NRC) of the National Academies. (2012). *Challenges and opportunities in the hydrologic sciences*. National Academy of Sciences Press, Washington, DC, 200p. Available online: https://doi.org/10.17226/13293

Nielsen, M. A. (2015). *Neural Networks and Deep Learning*, Determination Press. Available online: http://neuralnetworksanddeeplearning.com/index.html

Nilsson, C., Reidy, C. A., Dynesius, M., & Revenga, C. (2005). Fragmentation and flow regulation of the world's large river systems. *Science*, 308, 405-408.

Nippgen, F., McGlynn, B. L., Marshall, L. A., & Emanuel, R. E. (2011). Landscape structure and climate influences on hydrologic response. *Water Resources Research*, 47, W12528.

Nippgen, F., McGlynn, B. L., Emanuel, R. E., & Vose, J. M. (2016). Watershed memory at the Coweeta Hydrologic Laboratory: The effect of past precipitation and storage on hydrologic response. *Water Resources Research*, 52, 1673-1693.

Nippgen, F., McGlynn, B. L., Emanuel, R. E. (2015). The spatial and temporal evolution of contributing areas. *Water Resources Research*, 51(6), 4550-4573.

Ogden, F. L., Raj, P. N., Downer, C. W., Zahner, J. A. (2011). Relative importance of impervious area, drainage density, width function, and subsurface storm drainage on flood runoff from an urbanized catchment. *Water Resources Research*, 47, W12503.

O'Gorman P. A. & Schneider, T. (2009). Scaling of precipitation extremes over a wide range of climates simulated with an idealized GCM. *Journal of Climatology*, 22, 5676–85.

Oki, T., & Kanae, S. (2006). Global hydrological cycles and world water resources, *Science*, 313, 1068-1072.

Pedregosa, F., Varoquaux, G., Gamfort, A., Michel, V., Thirion, B., Grisel, O. et al. (2011). Scikit-learn: Machine Learning in Python. *Journal of Machine Learning Research*, 12, 2825-2830.

Piao, S., Friedlingstein, P., Ciais, P., de Noblet-Ducoudre, N., Labat, D., & Zaehle, S. (2007). Changes in climate and land use have a larger direct impact than rising CO2 on global river runoff trends. *Proceedings of the National Academies of Science*, 104, 15242-15247.

Pitman, A. J. (2003). The evolution of, and revolution in, land surface schemes designed for climate models. *International Journal of Climatology*, 23, 479-510.

Postel, S. L., Daily, G. C., & Ehrlich, P. R. (1996). Human appropriation of renewable fresh water. *Science*, 271, 785-788.

Python Software Foundation. (2018). Python Language Reference, version 3.7.1. Available online: http://www.python.org/.

R Core Team. (2017). R: A language and environment for statistical computing. R Foundation for Statistical Computing, Vienna, Austria. Available online: https://www.R-project.org/.

Raghavendra, S. N., & Deka, P. C. (2014). Support vector machine applications in the field of hydrology: A review. *Applied Soft Computing*, 19, 372-386.

Ramseyer, C. A., & Mote, T. L. (2018). Analysing regional climate forcing on historical precipitation variability in Northeast Puerto Rico. *International Journal of Climatology*, 38, e224-e236.

Ribeiro, M. T., Singh, S., & Guestrin, C. (2018). “Why Should I Trust You? Explaining the Predictions of Any Classifier”. *KDD '16 Proceedings of the 22nd ACM SIGKDD International Conference on Knowledge Discovery and Data Mining*, San Francisco, California, p1135-1144.

Rice, J. S., Emanuel, R. E., Vose, J. M., & Nelson, S. A. C. (2015). Continental U.S. streamflow trends from 1940 to 2009 and their relationships with watershed spatial characteristics. *Water Resources Research*, 51, 6262-6275.

Rice, J. S., Emanuel, R. E., & Vose, J. M. (2016). The influence of watershed characteristics on spatial patterns of trends in annual scale streamflow variability in the continental U.S. *Journal of Hydrology*, 540, 850-860.

Rice, J. S., & Emanuel, R. E. (2017). How are streamflow responses to the El Nino Southern Oscillation affected by watershed characteristics? *Water Resources Research*, 53, 4393-4406.

Rice, J. S., & Emanuel, R. E. (2019). Ecohydrology of interannual changes in watershed storage. *Water Resources Research*, 55, 2019WR025164.

Rinaldo, A., Vogel, G. K., Rigon, R., & Rodriguez-Iturbe, I. (1995). Can one gauge the shape of a basin? *Water Resources Research*, *31*, 1119-1127.

Riveros-Iregui, D. A., McGlynn, B. L., Emanuel, R. E., & Epstein, H. E. (2012). Complex terrain leads to bidirectional responses of soil respiration to inter-annual water availability, *Global Change Biology*, 18, 749-756.

Rodriguez-Iturbe, I., & Valdes, J. B. (1979). The geomorphic structure of hydrologic response. *Water Resources Research*, *15*, 1409-1420.

Rodriguez-Iturbe, I. (2000). Ecohydrology: A hydrologic perspective of climate-soil-vegetation dynamics. *Water Resources Research*, 36, 3-9.

Rolnick, D., & Tegmark, M. (2017, preprint). The power of deeper networks for expressing natural functions. Available online: https://arxiv.org/abs/1705.05502.

Reyes, W. M., Epstein, H. E., Li, X., McGlynn, B. L., Riveros-Iregui, D. A., Emanuel, R. E. (2017). Complex terrain influences ecosystem carbon responses to temperature and precipitation. *Global Biogeochemical Cycles*, 31, 1306-1317.

Saia, S. M., Suttles, K. M., Cutts, B. B., Emanuel, R. E., Martin, K. L, Wear, D. N., et al. (2019). Applying Climate Change Risk Management Tools to Integrate Streamflow Projections and Social Vulnerability. *Ecosystems*, in press.

Schmidhuber, J. (2015). Deep learning in neural networks: An overview, *Neural Networks*, 61, 85-117.

Schoof, J. T. (2013). Statistical Downscaling in Climatology. Geography Compass, 7, 249-265.

Seager, R., & Vecchi, G. A. (2010). Greenhouse warming and the 21st century hydroclimate of southwestern North America. *Proceedings of the National Academies of Science*, 107, 21277-21282.

Sellers, P. J., Bounoua, L., Collatz, G. J., Randall, D. A., Dazlich, D. A., et al. (1996). Comparison of radiative and physiological effects of doubled atmospheric CO2 on climate. *Science*, 271, 1402-1406.

Shen, C. (2018). A trans-disciplinary review of deep learning research and its relevance for water resources scientists. *Water Resources Research*, 54, 8558-8593.

Shen, C., Laloy, E. Elshorbagy, A. Albert, A., Bales, J. et al. (2018). HESS Opinions: Incubating deep-learning-powered hydrologic science advances as a community. Hydrological and Earth Systems Sciences, 22, 5639-5656.

Sheridan, S. C., & Lee, C. C. (2011). The self-organizing map in synoptic climatological research. Progress on Physical Geography, 35, 109-119.

Srinivasan, V., Konar, M., & Sivapalan, M. (2017). A dynamic framework for water security. *Water Security*, 1, 12-20.

Srivastava, N., Hinton, G., Krizhevsky, A., Sutskever, I., & Salakhutdinov, R. (2014). Dropout: A simple way to prevent neural networks from overfitting. *Journal of Machine Learning Research*, 15, 1929-1958.

Sutskever, I., Martens, J., Dahl, G., & Hinton, G. (2013). On the importance of initialization and momentum in deep learning. *Proceedings of the 30th International Conference on Machine Learning*, 28, 1139-1147. Available online: http://proceedings.mlr.press/v28/sutskever13.html.

Suttles, K. M., Singh, N. K., Vose, J. M., Martin, K. L., Emanuel, R. E., Coulston, J. W., et al. 2018. Assessment of hydrologic vulnerability to urbanization and climate change in a rapidly changing watershed in the Southeast U.S. *Science of the Total Environment*, 645, 806–16.

Tang, Q., & Lettenmaier, D. P. (2012). 21st century runoff sensitivities of major global river basins. *Geophysical Research Letters*, 39, L06403.

Tao, B., Tian, H., Ren, W., Yang, J., Yang, Q., He, R., Cai, W., & Lohrenz, S. (2014). Increasing Mississippi River discharge throughout the 21st century influenced by changes in climate, land use, and atmospheric CO2. *Geophysical Research Letters*, 41, 4978-4986.

Taylor, K. E., Stouffer, R. J., & Meehl, G. A. (2012). An overview of CMIP5 and the experimental design. *Bulletin of the American Meteorological Society*, 93, 485-498.

Terando, A. J., Costanza, J., Belyea, C., Dunn, R. R., McKerrow, A., & Collazo, J. A. (2014). The southern megalopolis: Using the past to predict the future of urban sprawl in the Southeast U.S. *PLoS One*, 9:e102261.

Trigo, R. M., & Palutikof, J. P. (1999). Simulation of daily temperatures for climate change scenarios over Portugal: a neural network model approach. *Climate Research*, 13, 45-59.

Tripathi, M. P., Raghuwanshi, N. S., Rao, G. P. (2006). Effect of watershed subdivision on simulation of water balance components. *Hydrological Processes*, 20, 1137-1156.

Udall, B., & Overpeck, J. (2017). The twenty-first century Colorado River hot drought and implications for the future. *Water Resources Research*, 53, 2404– 2418.

United States Department of Agriculture Forest Service (USFS). (2012). *Future scenarios: a technical document supporting the Forest Service 2010 RPA Assessment*. General Technical Report RMRS-GTR-272. USFS, Rocky Mountain Research Station, Fort Collins, CO. 34p.

United States Geologic Survey (USGS). (2013). National Elevation Dataset (NED) - Conterminous United States 100 Meter Resolution Albers Projection. Available online: https://nationalmap.gov/small_scale/mld/elev100.html

van der Walt, S., Colbert, S. C., & Varoquaux, G. (2011). The NumPy Array: A Structure for Efficient Numerical Computation. *Computing in Science & Engineering*, 13: 22-30.

Villarini, G., & Smith, J. A. (2010). Flood peak distributions for the eastern United States. *Water Resources Research*, 46, W06504.

Virtanen, P., Gommers, R., Oliphant, T. E., Haberland, M., Reddy, T. Cournapeau, D. et al. (2019, preprint). SciPy 1.0–Fundamental Algorithms for Scientific Computing in Python. Available online: https://arxiv.org/abs/1907.10121

Vorosmarty, C. J., Green, P., Salisbury, J., & Lammers, R. B. (2000). Global water resources: Vulnerability from climate change and population growth. *Science*, 289, 284-288.

Vose, J. M. (2018). Forest and Water in the 21st Century: A Global Perspective. *Forestry*, 117(1), 80–85.

Wagener, T., Sivapalan, M., Troch, P., & Woods, R. (2007). Catchment classification and hydrologic similarity. *Geography Compass*, 1, 901–931.

Walsh, J., Wuebbles, D., Hayhoe, K., Kossin, J., Kunkel, K., Stephens, G., et al. (2014). *Ch. 2: Our Changing Climate. Climate Change Impacts in the United States*: The Third National Climate Assessment. (eds.) JM Melillo, TC Richmond, and GW Yohe. United States Global Change Research Program, Washington, DC. pp 19-67.

Wear, D. N. (2013). *Chapter 4: Forecasts of Land Uses*. The Southern Forest Futures Project: Technical Report. (eds.) DN Wear and JG Greis. General Technical Report SRS-179. United States Department of Agricultural Forest Service Research and Development, Southern Research Station, Ashville, NC. pp 45-71.

Weiler, M., McGlynn, B. L., McGuire, K. J., and McDonnell, J. J. (2003). How does rainfall become runoff? A combined tracer and runoff transfer function approach. *Water Resources Research*, 39, 1315.

Wilby, R. L., & Wigley, T. M. L. (1997). Downscaling general circulation model output: a review of methods and limitations. *Progress in Physical Geography*, 21, 530-548.

Woodhouse, C. A., Pederson, G. T., Morino, K., McAfee, S. A., & McCabe, G. J. (2016). Increasing influence of air temperature on upper Colorado River streamflow. *Geophysical Research Letters*, 43, 2174-2181.

Worland, S. C., Steinschneider, S., Asquith, W., Knight, R., & Wieczorek, M. (2019). Prediction and inference of flow duration curves using multioutput neural networks. *Water Resources Research*, 55, 6850-6868.

Fry, J. A., Xian, G., Jin, S., Dewitz, J. A., Homer, C. G., Yang, L. et al. (2012). Completion of the 2006 National Land Cover Database Update for the Conterminous United States. *Photogrammetric Engineering and Remote Sensing*, 77, 858-864.

Zhang, X., Tang, Q., Zhang, X., & Lettenmaier, D. P. (2014). Runoff sensitivity to global mean temperature change in the CMIP5 models. *Geophysical Research Letters*, 41, 5492-5498.

Zhao, M., & Running, S. W. (2010). Drought-induced reduction in global terrestrial net primary production from 2000 through 2009. *Science*, 329, 940-943.

Journal of Advances in Modeling Earth Systems

Supporting Information for

Improved Accuracy of Watershed-Scale General Circulation Model

Runoff Using Deep Neural Networks

Joshua S. Rice[1], Sheila M. Saia[1], Ryan E. Emanuel[1,2]

Department of Forestry and Environmental Resources, North Carolina State University, Raleigh, NC 27695, USA

Center for Geospatial Analytics, North Carolina State University, Raleigh, NC 27695, USA

Contents of this file

Figures S1-S10, Table S1-S6

Additional Supporting Information

Data and scripts associated with this publication are available on GitHub at [insert link here upon manuscript acceptance] and Zenodo (DOI: [insert link here upon manuscript acceptance]).

Introduction

This manuscript supporting information document includes conceptual diagrams showing the architecture of machine learning models used in this study, deep neural network (DNN) model inputs and outputs, and the semi-random training and test set split proportions. We included a figure showing the location and region of watersheds used in this study and several model testing figures. In addition to figures, we included a table describing the DNN input variables and tables with model assessment metrics for non-reference and reference test set results, Q10 and Q90 test set results, and ecoregional results.

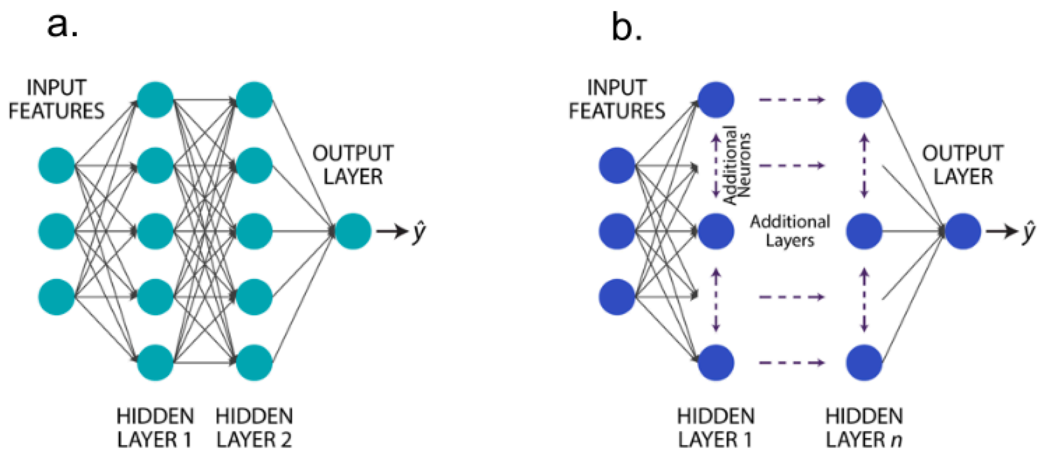

Figure S1. (a) Architecture of a simple artificial neural network (ANN) with two hidden layers and a limited number of neurons (cyan circles). (b) Architecture of a more complex deep neural network (DNN) with several hidden layers and neurons (blue circles).

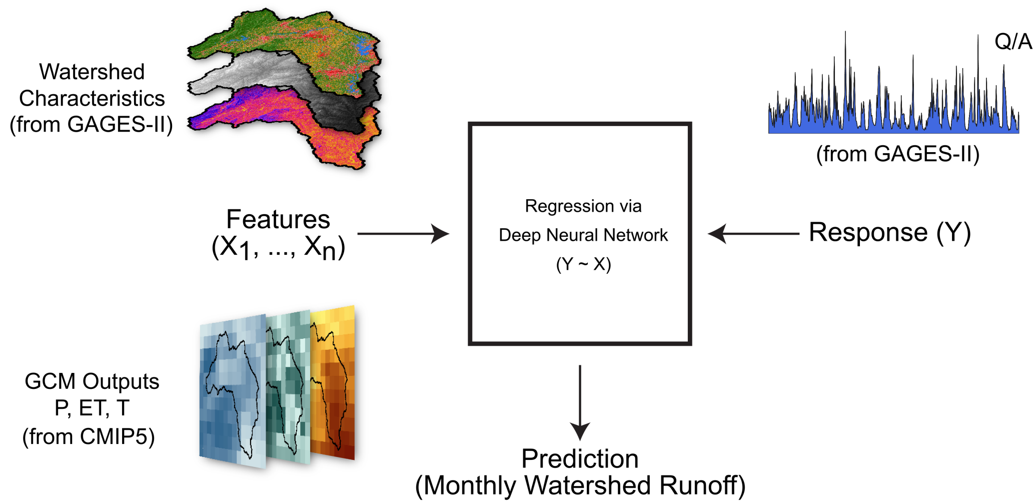

Figure S2. Conceptual overview of how we trained a deep neural network (DNN) to predict monthly watershed-scale runoff. The DNN feature variables included watershed characteristics and monthly, gridded, downscaled Coupled Model Intercomparison Project Phase 5 (CMIP5) general circulation model (GCM) precipitation (P), evapotranspiration (ET), and temperature (T). We also used several abiotic and biotic watershed characteristics from the Gages for Evaluating Streamflow version II (GAGES-II) dataset (Falcone et al., 2010). Observed monthly runoff—equal to streamflow at the gauging station (Q) divided by watershed area (A)—was the response variable.

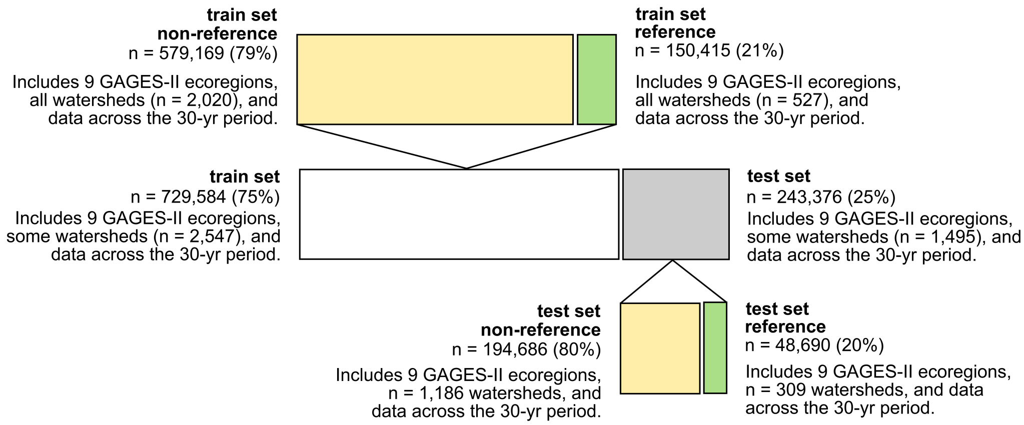

Figure S3. Breakdown of observed monthly runoff (i.e., DNN response) data distribution between train and test sets. Yellow represents data from non-reference watersheds and green represents data from reference watersheds. Note that the sum of watersheds does not add to n = 2,731 between the train and test set because of the semi-random sampling grouped by time; some watersheds are represented in both the training and test set but their time points differ. Abbreviations: Geospatial Attributes of Gages for Evaluating Streamflow version II (GAGES-II; Falcone et al., 2010).

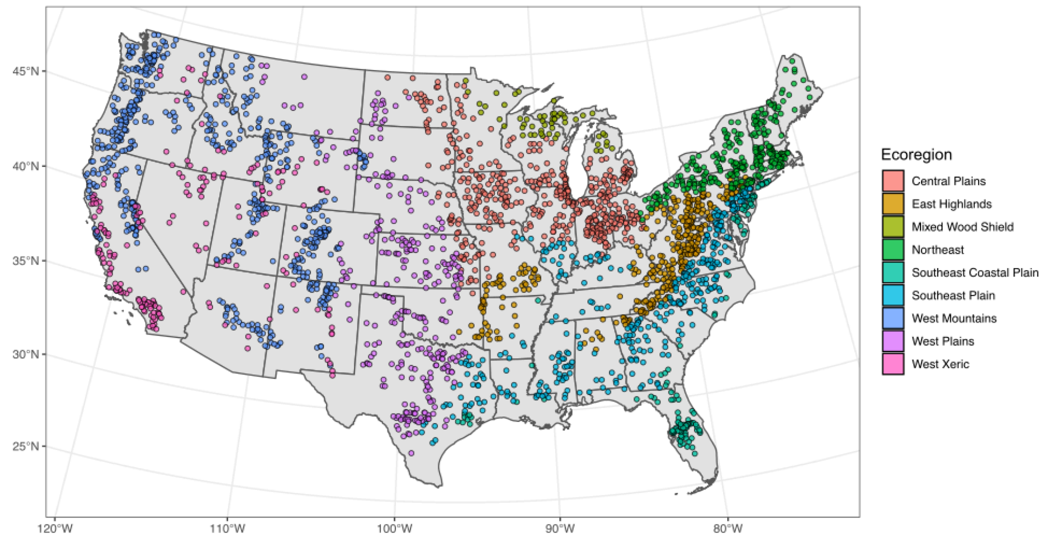

Figure S4. Geospatial Attributes of Gages for Evaluating Streamflow version II (GAGES-II; Falcone et al., 2010) watershed ecoregions used in this study.

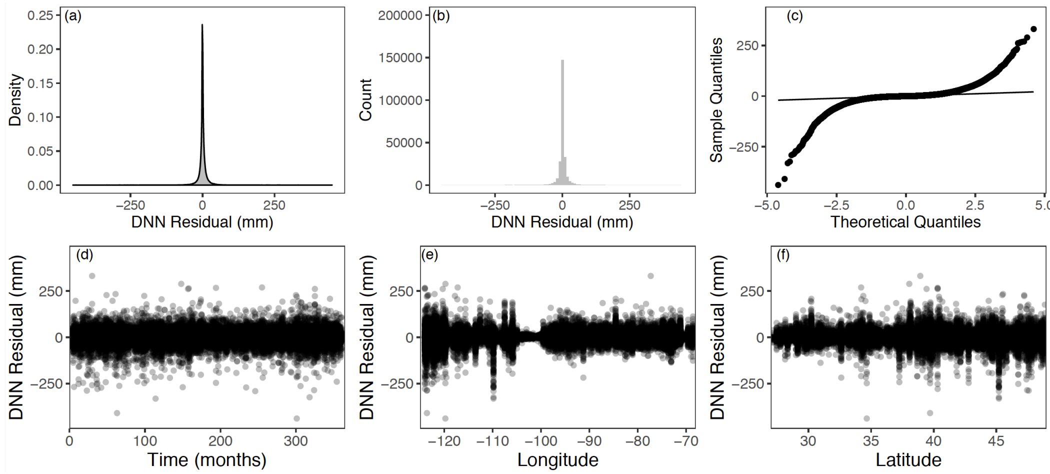

Figure S5. Deep neural network (DNN) test set results showing (a) DNN residual density distribution, (b) DNN residual histogram, (c) DNN qq-plot with random normal line-of-best-fit, (d) DNN residuals versus time, (e) DNN residuals versus longitude of the watershed centroid, and (f) DNN residuals versus latitude of the watershed centroid.

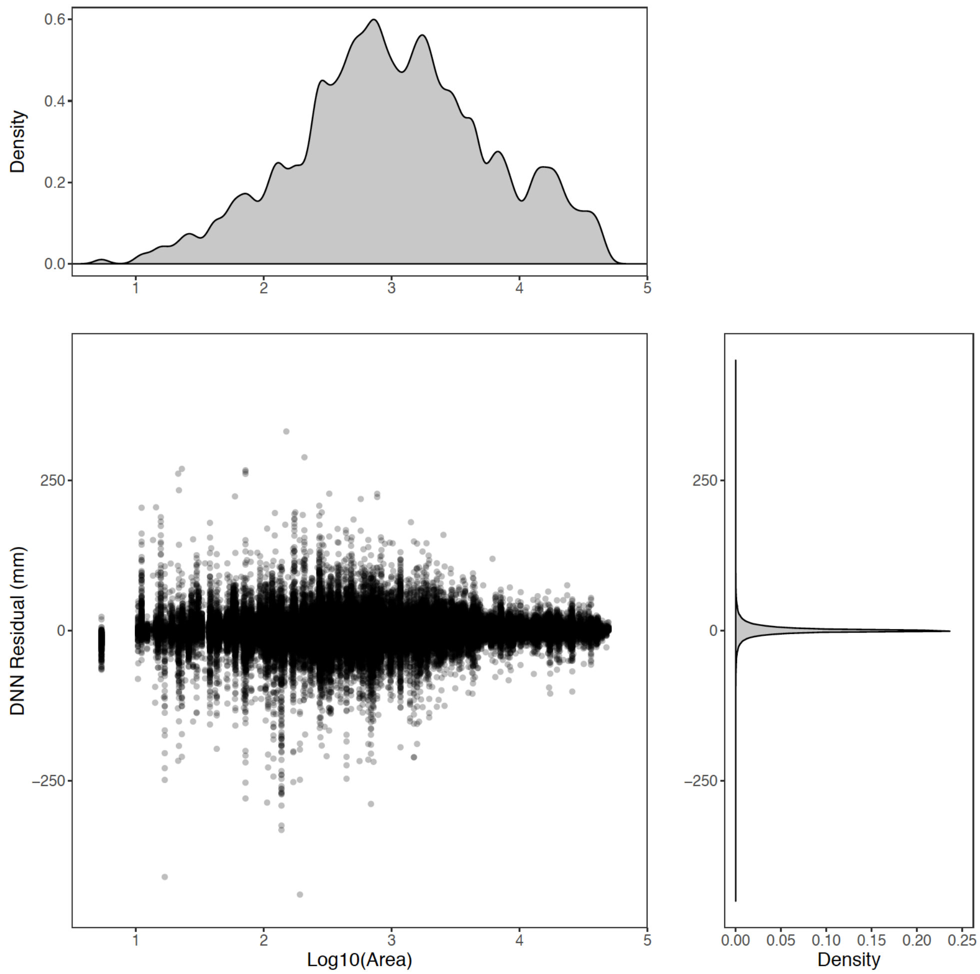

Figure S6. Deep neural network (DNN) test set results showing DNN residuals versus logged (base 10) watershed area (center panel). Top panel shows the distribution of logged watershed areas and right-side panel shows the distribution of DNN residuals (i.e., the same as Figure S5a).

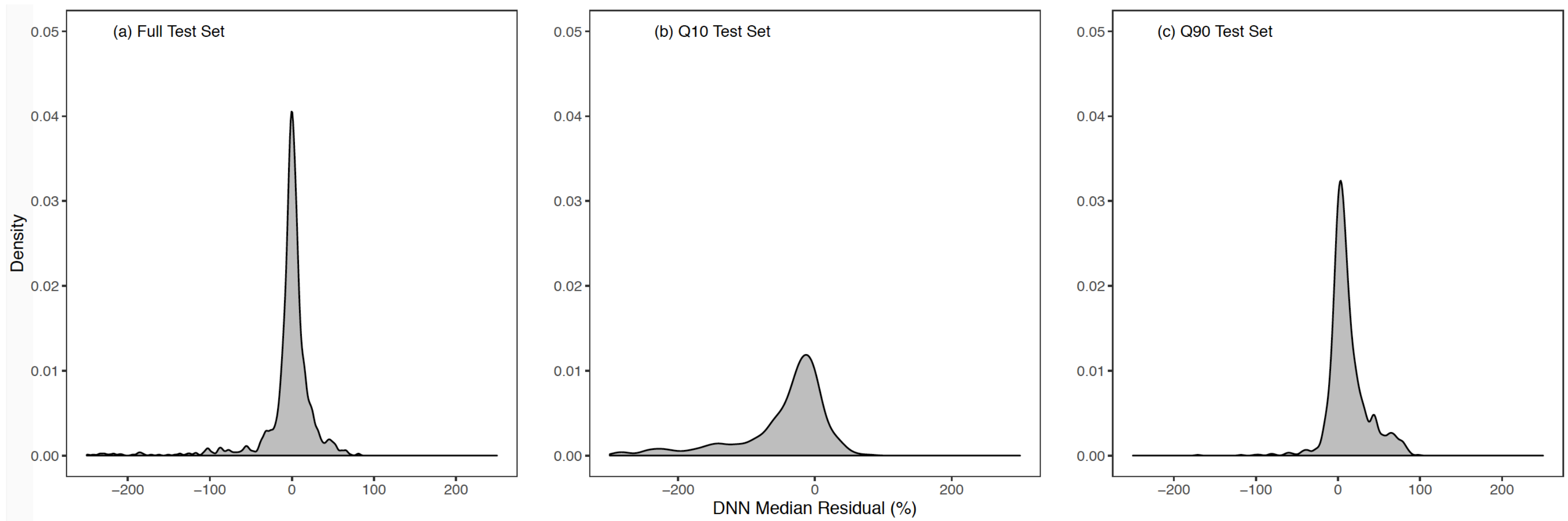

Figure S7. Deep neural network watershed median residual density plots for the (a) full test set, (b) Q10 event test set, and (c) Q90 event test set.

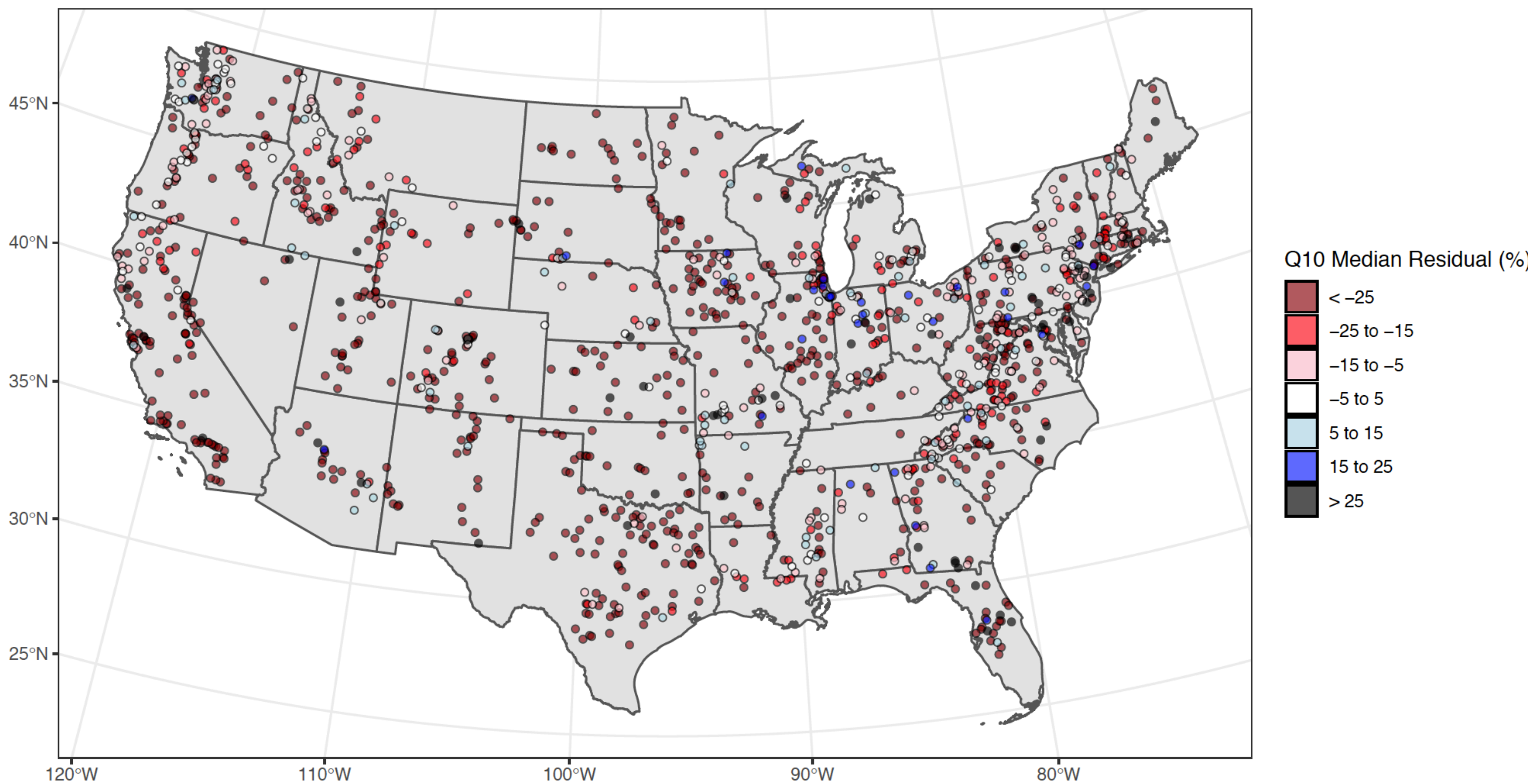

Figure S8. Deep neural network test set Q10 event median watershed residuals expressed as a percent relative to observations. Point location represents the watershed centroid.

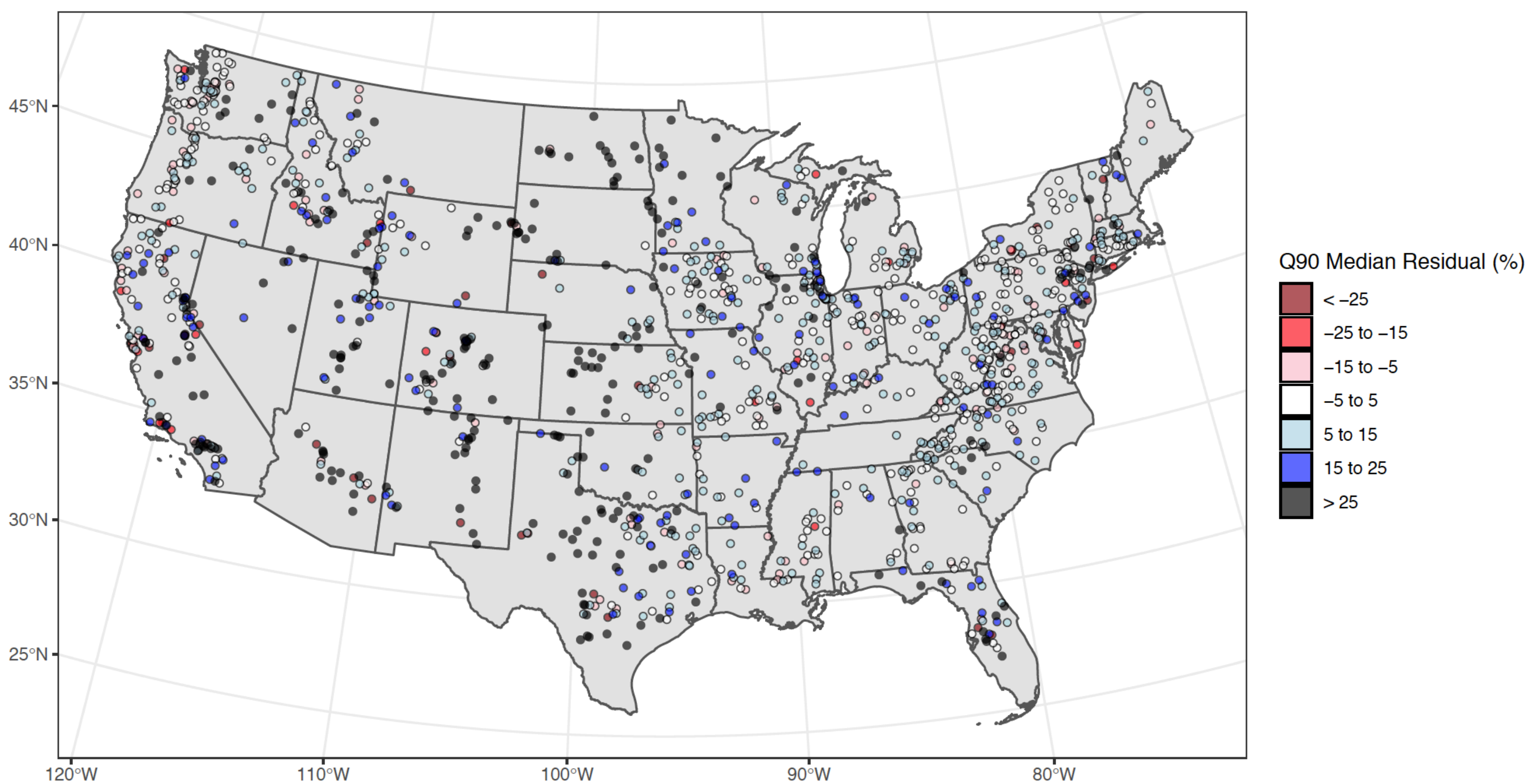

Figure S9. Deep neural network test set Q90 event median watershed residuals expressed as a percent relative to observations. Point location represents the watershed centroid.

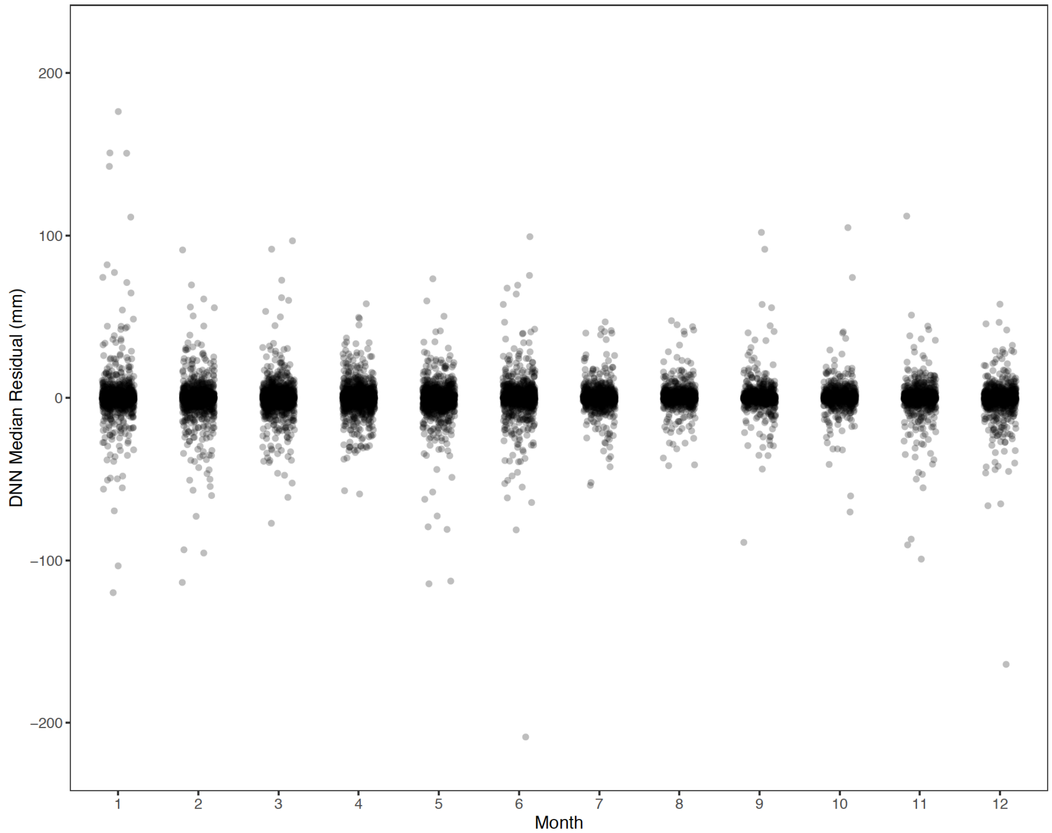

Figure S10. Deep neural network median watershed residuals grouped by month.

January is equivalent to 1 and December is equivalent to 12.

Table S1. List of watershed characteristics included as deep neural network input variables (i.e., features). Abbreviations: Coupled Model Intercomparison Project Phase 5 (CMIP5; Maurer et al., 2007; Taylor et al., 2012), United States Geological Survey Geospatial Attributes of Gages for Evaluating Streamflow version II (USGS GAGE-II; Falcone et al., 2010), digital elevation model (DEM), United States Geologic Survey National Elevation Dataset (USGS NED; USGS, 2013).

Number	Variable Name	Description	Units	Data Source
1	LAG0_P	Watershed aerially averaged total monthly precipitation for each month	mm	CMIP5 output
2	LAG1_P	Watershed aerially averaged one month lagged total monthly precipitation for each month	mm	CMIP5 output
3	LAG2_P	Watershed aerially averaged two month lagged total monthly precipitation for each month	mm	CMIP5 output
4	LAG3_P	Watershed aerially averaged three month lagged total monthly precipitation for each month	mm	CMIP5 output
5	LAG0_ET	Watershed aerially averaged total monthly evapotranspiration for each month	mm	CMIP5 output
6	LAG1_ET	Watershed aerially averaged one month lagged total monthly evapotranspiration for each month	mm	CMIP5 output
7	LAG2_ET	Watershed aerially averaged two month lagged total monthly evapotranspiration for each month	mm	CMIP5 output
8	LAG3_ET	Watershed aerially averaged three month lagged total monthly evapotranspiration for each month	mm	CMIP5 output
9	LAG0_T	Watershed aerially averaged mean monthly surface temperature for each month	degrees C	CMIP5 output
10	LAG1_T	Watershed aerially averaged one month lagged mean monthly surface temperature for each month	degrees C	CMIP5 output
11	LAG2_T	Watershed aerially averaged two month lagged mean monthly surface temperature for each month	degrees C	CMIP5 output
12	LAG3_T	Watershed aerially averaged three month lagged mean monthly surface temperature for each month	degrees C	CMIP5 output
13	PPTAVG_BASIN	Average annual precipitation for the watershed from 800m PRISM data for 30-year record (1971-2000)	cm	USGS GAGES-II
14	T_AVG_BASIN	Average annual air temperature for the watershed from 2km PRISM data for 30-year record (1971-2000)	degrees C	USGS GAGES-II
15	WD_BASIN	Watershed mean annual number of days of measurable precipitation from 2km PRISM data from 30-year record (1961-1990)	days	USGS GAGES-II
16	SNOW_PCT_PRECIP	Mean snow percent of total precipitation estimate for period 1901-2000, 1km grid	%	USGS GAGES-II
17	LAT_CENT	Latitude of the watershed geographic centroid	decimal degrees	USGS GAGES-II
18	LONG_CENT	Longitude of the watershed geographic centroid	decimal degrees	USGS GAGES-II
19	ELEV_MEAN_M_BASIN	Mean watershed elevation	m	USGS GAGES-II
20	ELEV_STD_M_BASIN	Standard deviation of watershed elevation	m	USGS GAGES-II
21	RRMEAN	Mean watershed relief ratio, which is equal to the difference between the maximum and minimum watershed elevation over the total length of streams in the watershed	NA	USGS GAGES-II
22	RRMEDIAN	Median watershed relief ratio	N/A	USGS GAGES-II
23	SLOPE_PCT	Mean watershed percent slope	%	USGS GAGES-II
24	SLOPE_SD	Standard deviation of watershed slope	%	Computed in ArcGIS from a 100 m DEM from the USGS NED
25	UAA_MEAN	Mean watershed upslope accumulation area (UAA) after scaling UAA values from 0 - 1 using maximum scaling	m	Computed in ArcGIS from a 100 m DEM from the USGS NED
26	UAA_SD	Standard deviation of watershed upslope accumulation area (UAA) after scaling UAA values from 0 - 1 using maximum scaling.	m	Computed in ArcGIS from a 100 m DEM from the USGS NED
27	BAS_COMPACTNESS	Watershed compactness ratio, which is equal to watershed area divided by the watershed perimeter squared times 100; the higher the compactness ratio, the more compact the watershed shape	N/A	USGS GAGES-II

Continues on next page.

Number	Variable Name	Description	Units	Data Source
28	TOPWET	Watershed topographic wetness index, which is equal to ln(UAA/S); where "ln" is the natural log, "a" is UAA at a given point and "S" is the slope at that point	N/A	USGS GAGES-II
29	MAINSTEM_SINUOUSITY	Sinuosity of mainstem stream line, from GAGES-II delineation of mainstem stream lines. Equal to the curvilinear length of the mainstem stream line divided by the straight-line distance between the end points of the line	N/A	USGS GAGES-II
30	STREAMS_KM_SQ_KM	Watershed stream density, relative to watershed area	km per sq km	USGS GAGES-II
31	ROADS_KM_SQ_KM	Watershed road density, relative to watershed area	km per sq km	USGS GAGES-II
32	CLAYAVE	Watershed average percent of clay content in soils	%	USGS GAGES-II
33	SANDAVE	Watershed average percent of sand content in soils	%	USGS GAGES-II
34	SILTAVE	Watershed average percent of silt content in soils	%	USGS GAGES-II
35	ROCKDEPAVE	Watershed average percent of total soil thickness	in	USGS GAGES-II
36	DEVNLCD06	Watershed percent "developed" from the 2006 NLCD. Sum of classes 21, 22, 23, and 24	%	USGS GAGES-II
37	FORESTNLCD06	Watershed percent "forest" from the 2006 NLCD. Sum of classes 41, 42, and 43	%	USGS GAGES-II
38	PLANTNLCD06	Watershed percent "planted/cultivated" from the 2006 NLCD. Sum of classes 81 and 82	%	USGS GAGES-II
39	GRASSNLCD06	Watershed percent “grassland” from the 2006 NLCD. Includes class 71	%	USGS GAGES-II
40	WOODYWETNLCD06	Watershed percent Woody Wetlands (class 90) from 2006 NLCD	%	USGS GAGES-II
41	EMERGWETNLCD06	Watershed percent Emergent Wetlands (class 96) from 2006 NLCD	%	USGS GAGES-II
42	RIP100_DEV	Riparian 100 m buffer "developed" from the 2006 NLCD. Sum of classes 21, 22, 23, and 24. Buffer area spans 100 m on each side of stream centerline for all streams in watershed	%	USGS GAGES-II
43	RIP100_FOREST	Riparian 100 m buffer "forest", 2006 era NLCD. Sum of classes 41, 42, and 43. Buffer area spans 100 m on each side of stream centerline for all streams in watershed	%	USGS GAGES-II
44	RIP100_PLANT	Riparian 100 m buffer "planted/cultivated" from the 2006 NLCD. Sum of classes 81 and 82. Buffer area spans 100 m on each side of stream centerline for all streams in watershed	%	USGS GAGES-II
45	RIP100_71	Riparian 100 m buffer “grassland” from the 2006 NLCD. Includes class 71, buffer area spans 100 m on each side of stream centerline for all streams in watershed	%	USGS GAGES-II
46	RIP100_90	Watershed percent Woody Wetlands in 100m riparian 100m buffer from 2006 NLCD	%	USGS GAGES-II
47	RIP100_95	Watershed percent Emergent Wetlands in 100m riparian 100m buffer from 2006 NLCD	%	USGS GAGES-II
48	BFI_AVG	Watershed average base flow index (BFI), equal to the ratio of base flow to total streamflow, ranges from 0% to 100%	%	USGS GAGES-II
49	CONTACT	Subsurface flow contact time index, which estimates the number of days that infiltrated water resides in the saturated subsurface zone of the basin before discharging into the stream	days	USGS GAGES-II
50	MTDEPAVE	Watershed mean depth to seasonally high water table	ft	USGS GAGES-II
51	CAL_MONTH_1	Calendar month (0 for non-January month, 1 for January)	N/A	This study
52	CAL_MONTH_2	Calendar month (0 for non-February month, 1 for February)	N/A	This study
53	CAL_MONTH_3	Calendar month (0 for non-March month, 1 for March)	N/A	This study
54	CAL_MONTH_4	Calendar month (0 for non-April month, 1 for April)	N/A	This study
55	CAL_MONTH_5	Calendar month (0 for non-May month, 1 for May)	N/A	This study
56	CAL_MONTH_6	Calendar month (0 for non-June month, 1 for June)	N/A	This study
57	CAL_MONTH_7	Calendar month (0 for non-July month, 1 for July)	N/A	This study
58	CAL_MONTH_8	Calendar month (0 for non-August month, 1 for August)	N/A	This study
59	CAL_MONTH_9	Calendar month (0 for non-September month, 1 for September)	N/A	This study
60	CAL_MONTH_10	Calendar month (0 for non-October month, 1 for October)	N/A	This study
61	CAL_MONTH_11	Calendar month (0 for non-November month, 1 for November)	N/A	This study
62	CAL_MONTH_12	Calendar month (0 for non-December month, 1 for December)	N/A	This study

Table S2. Model performance comparisons for monthly Q10 and Q90 events in the test set. Abbreviations: Generalized Circulation Model (GCM), median absolute error (MAE), Pearson's correlation coefficient (PCC), support vector machine (SVM), extreme gradient boosting (XGBoost), artificial neural network (ANN), and deep neural network (DNN). MAE and PCC are reported with the lower and upper 95% confidence intervals in parentheses.

	Q10 Test Set				Q90 Test Set			
Method	Bias (mm)	Slope	MAE (%)	PCC	Bias (mm)	Slope	MAE (%)	PCC
GCM Runoff	1.80	0.43	149.05 (144.55, 153.99)	0.506 (0.479, 0.534)	35.34	0.82	35.36 (34.93, 35.97)	0.767 (0.757, 0.779)
Monthly Normal Runoff	-1.11	0.41	293.91 (286.79, 301.05)	0.792 (0.780. 0.803)	26.82	1.41	48.45 (48.02, 48.86)	0.871 (0.865, 0.877)
Linear Ridge Regression	7.83	8.29E-15	>1000	0.159 (0.152, 0.167)	125.36	8.81E+00	>1000	0.188 (0.178, 0.198)
SVM	-1.30	0.29	736 (718.27, 755.52)	0.555 (0.536, 0.573)	-15.63	1.93	42.67 (42.29, 43.02)	0.824 (0.816, 0.832)
XGBoost	0.85	0.56	125.58 (121.67, 129.42)	0.797 (0.785, 0.811)	13.62	1.06	25.63 (25.26, 25.97)	0.934 (0.930, 0.937)
ANN	0.91	0.63	82.44 (80.38, 84.81)	0.703 (0.681, 0.724)	10.02	1.29	32.00 (31.61, 32.39)	0.908 (0.904, 0.912)
DNN	0.52	0.73	50.87 (49.49, 52.26)	0.880 (0.869, 0.892)	12.94	0.94	15.96 (15.66, 16.27)	0.956 (0.953, 0.958)

Table S3. Model performance comparisons for non-reference and reference watersheds in the test set. Abbreviations: Generalized Circulation Model (GCM), Pearson's correlation coefficient (PCC), support vector machine (SVM), extreme gradient boosting (XGBoost), artificial neural network (ANN), and deep neural network (DNN). PCC is reported with the lower and upper 95% confidence intervals in parentheses.

	Non-reference Test Set			Reference Test Set		
Method	Bias (mm)	Slope	PCC	Bias (mm)	Slope	PCC
GCM Runoff	7.06	0.81	0.787 (0.781, 0.793)	9.02	0.93	0.841 (0.835, 0.848
Monthly Normal Runoff	0.08	1.01	0.795 (0.791, 0.799)	0.20	0.99	0.829 (0.823, 0.834)
Linear Ridge Regression	38.53	3.42E-14	0.164 (0.160, 0.168)	57.85	6.18E-14	0.126 (0.118, 0.133)
SVM	16.12	1.23	0.755 (0.750, 0.759)	23.46	1.45	0.792 (0.785, 0.797)
XGBoost	-0.08	1.01	0.920 (0.917, 0.922)	-0.34	1.02	0.948 (0.945, 0.950)
ANN	0.308	1.16	0.900 (0.897, 0.902)	-1.19	1.23	0.935 (0.932, 0.937)
DNN	2.36	0.94	0.954 (0.953, 0.957)	2.60	0.95	0.971 (0.969, 0.973)

Table S4. Modeled versus observed runoff bias comparisons by ecoregion for the test set. Abbreviations: Generalized Circulation Model (GCM), support vector machine (SVM), extreme gradient boosting (XGBoost), artificial neural network (ANN), and deep neural network (DNN).

Model	Central Plains	East Highlands	Mixed Wood Shield	Northeast	Southeast Coastal Plain	Southeast Plain	West Mountains	West Plains	West Xeric
GCM Runoff	1.96	7.98	13.55	8.07	3.23	2.79	13.56	0.55	2.63
Monthly Normal Runoff	-0.03	-0.03	0.04	-0.05	-0.30	-0.15	-0.08	-0.01	-0.10
Linear Ridge Regression	21.22	41.26	55.34	54.61	29.21	39.21	120.11	11.64	14.43
SVM	-20.46	-48.82	-11.48	-66.89	-14.97	-35.59	-18.87	-3.63	0.01
XGBoost	-0.62	-2.12	-0.24	-3.19	2.46	0.59	-0.41	-0.22	0.74
ANN	0.38	-1.24	5.28	-2.44	4.88	-0.25	1.31	0.69	1.33
DNN	1.46	1.85	1.98	0.83	7.31	1.82	2.49	0.84	1.97

Table S5. Modeled versus observed runoff slope comparisons by ecoregion for the test set. Abbreviations: Generalized Circulation Model (GCM), support vector machine (SVM), extreme gradient boosting (XGBoost), artificial neural network (ANN), and deep neural network (DNN).

Model	Central Plains	East Highlands	Mixed Wood Shield	Northeast	Southeast Coastal Plain	Southeast Plain	West Mountains	West Plains	West Xeric
GCM Runoff	1.07	0.95	1.01	1.02	0.76	0.96	0.81	0.76	0.56
Monthly Normal Runoff	1.01	1.00	1.00	1.00	1.01	1.01	0.99	0.99	1.03
Linear Ridge Regression	-5.01E-15	-4.82E-14	2.56E-13	5.41E-14	-7.75E-15	3.99E-14	1.88E-13	2.23E-14	1.37E-14
SVM	1.29	1.79	1.30	2.20	1.05	1.55	1.37	0.65	0.77
XGBoost	1.03	10.50	1.10	1.07	0.96	1.00	1.01	1.00	0.90
ANN	1.11	1.16	1.14	1.14	1.08	1.14	1.22	1.19	1.24
DNN	0.96	0.97	1.08	0.98	0.87	0.98	0.93	0.96	0.89

Table S6. Modeled runoff versus observed runoff Pearson's correlation coefficient comparisons by ecoregion for the test set. Abbreviations: Generalized Circulation Model (GCM), support vector machine (SVM), extreme gradient boosting (XGBoost), artificial neural network (ANN), and deep neural network (DNN).

Model	Central Plains	East Highlands	Mixed Wood Shield	Northeast	Southeast Coastal Plain	Southeast Plain	West Mountains	West Plains	West Xeric
GCM Runoff	0.81	0.83	0.58	0.81	0.68	0.86	0.80	0.74	0.73
Monthly Normal Runoff	0.56	0.66	0.84	0.70	0.61	0.60	0.86	0.60	0.66
Linear Ridge Regression	-0.06	-0.07	0.41	0.06	-0.07	0.08	0.42	0.17	0.07
SVM	0.73	0.78	0.53	0.69	0.56	0.77	0.78	0.58	0.59
XGBoost	0.88	0.91	0.85	0.88	0.77	0.90	0.95	0.84	0.84
ANN	0.88	0.91	0.72	0.88	0.79	0.90	0.92	0.78	0.80
DNN	0.94	0.96	0.83	0.94	0.80	0.95	0.97	0.91	0.90